An Investigation of Reliability of High Density Electronic Package-to-Board Interconnections from the Perspective of Solder Joint Metallurgy

Weiqun Peng

Dissertation for the degree of Doctor of Science in Technology to be presented with due permission of the Faculty of Electronics, Communications and Automation, for public examination and debate in Auditorium S4 at Aalto University School of Science and Technology (Espoo, Finland) on the 13th of December, 2010, at 12:00.

Abstract

The integration and miniaturization trend of the electronic packaging leads to much finer pitch of the device and package lead terminations. Several reliability concerns and issues that were previously not encountered are now surfacing. The objective of this thesis work is to investigate the reliability of the package-to-board interconnection from the perspective of solder joint metallurgy. It was carried out with several advanced packages such as CSP, WLCSP and leadless ceramic packages on organic laminate PWBs using tin-silver-copper based interconnection materials. The assemblies were subjected to several loading conditions and levels such as thermal, mechanical, and environmental stresses. As expected, the board level reliability (BLR) of electronic assemblies strongly depended on microstructure and morphology of the solder joints. Dispersion strengthening effect of the intermetallic compounds (IMCs), coarsening of the IMC particles, strain rate hardening, solder fatigue, and recrystallization of Sn grains in the highly stressed areas were observed. These were found to directly impact Pb-free solder joint reliability. Appropriate thermal aging can improve joint reliability up to 50% due to coarsening of the IMC particles. In addition, other factors such as dissolution of metals, interfacial reactions, IMC spalling, and cross interaction of surface materials on the two sides of the joints were also observed and discussed. The effects can be expressed as a series of interactive relationships: materials (pad surface materials and solder alloy composition) and/or soldering process lead to microstructure change in bulk solder and/or at interface, which in turn leads to joint reliability variation.

Preface

This thesis has been carried out at the Faculty of Electronics, Communications and Automation at Aalto University School of Science and Technology. I warmly thank my supervisor Professor Mervi Paulasto-Kröckel for the guidance, support, the valuable discussions and the thesis structure. Her enthusiasm and expertise truly inspired me.

I'm most grateful to my Professor emeritus Jorma Kivilahti, not only for his sound guidance, support and time, but also for introducing me to the world of materials, interconnection technologies and electronics manufacturing. His continuous reminding of the practical constrains and the applicability of this work prepared me for the practical soldering problems that I have encountered later on.

I wish to thank the co-authors of my publications Dr. Eduardo Monlevade, Dr. Marco Marques, Dr. Puligandla Viswanadham, Dr. Jianjun Wang, Dr. Wei Ren, Mr. Steve Dunford, and Dr. Stephen Quander for their contributions and willingness for discussion at any time. Special thanks to Dr. Puligandla Viswanadham for his comments and feedbacks to the thesis.

I am also grateful to my former Nokia managers Dr. Jukka Rantala, Dr. Arni Kujala, Dr. Ramin.Vatanparast and Dr. Tommi Reinikainen for their constant support and encouragement. I also thank my Texas Instruments managers Mr. David Walter, Mrs. Laura McLaughlin and Mr. Dan Corum for their kind understanding and great support.

I thank Mrs. Pia.Holmberg, Dr. Vesa Vuorinen and Dr. Toni Mattila in the laboratory of Electronics Integration and Reliability in Aalto University for their constant help for so many years in administration and other things related with my PhD study.

I dedicate this thesis to my father and greatly thank my mother for their continuous support and love.

Finally I express my humble gratitude to my husband Dr. Kejun Zeng for his endless love and support. No words will ever be enough to thank him properly. And lastly, huge hugs for our lovely son Peng Zeng for endless encouragement and understanding.

Dallas, Dec. 2010
Weiqun Peng

Contents

List of publications

Publication I   Weiqun Peng and Marco E. Marques, "Effect of Thermal Aging on Drop Performance of Chip Scale Packages with SnAgCu Solder Joints on Cu Pads", *Journal of Electronic Materials,* **36**, 12, (2007), pp. 1679-1690.

Publication II   Weiqun Peng, Eduardo Monlevade, and Marco E. Marques, "Effect of Thermal Aging on the Interfacial Structure of SnAgCu Solder Joints on Cu", *Microelectronics Reliability*, **47**, 12, (2007), pp. 2161-2168.

Publication III   Eduardo Monlevade and Weiqun Peng, "Failure Mechanisms and Crack Propagation Paths in Thermally Aged Pb-free Solder Interconnects", *Journal of Electronic Materials,* **36**, 7, (2007), pp. 783-797.

Publication IV   Weiqun Peng, Steve Dunford, Puligandla Viswanadham, and Stephen Quander, "Microstructure and Performance Implications of Gold in Sn-Ag-Cu-Sb Interconnections", *The Proceedings of the 53rd Electronic Components and Technology Conference*, San Diego, CA, USA, May 30 - June 2, 2003, IEEE, (2003), pp. 809-815.

Piblication V   Weiqun Peng, "An Investigation of Sn Pest in Pure Sn and Sn-based Solders", *Microelectronics Reliability*, **49**, 1, (2009), pp. 86-91.

Publication VI   Jianjun Wang, Weiqun Peng, and Wei Ren, "Power Amplifier (PA) Transistors Fatigue Life Prediction under Thermo-Mechanical Cyclic Loading", *The Proceedings of EUROSIME 2006*, Como, Italy, April 23-26, 2006, IEEE, (2006), pp. 1-8.

The research program was planned and the theoretical aspects were discussed by the author with the co-authors. The author as a project manager in Nokia planned the experimental work and carried out the statistical analyses, failure analyses and theoretical explanations of the reliability data. The author wrote the manuscript, which has been discussed in detail with the co-authors. The drop test was carried out by Cleber Pagliosa and Jose´ Erick Lima, and mechanical modeling by co-author Dr. Jianjun Wang. In addition to the six publications, some additional research results from author's licentiate thesis are also included.

List of abbreviations and symbols

A	Ampere
Ag	Silver
Al	Aluminum
at. %	Atomic percent
Au	Gold
BCT	Body Centered Tetragonal
BGA	Ball Grid Array
Bi	Bismuth
BLR	Board Level Reliability
CSP	Chip Scale Package
CTE	Coefficient Thermal Expansion
Cu	Copper
D	Diffusion coefficient
DTA	Differential Thermal Analysis
EDX	Energy Dispensive X-Ray
FCBGA	Flip Chip Ball Grid Array
FCC	Face Centered Cubic
FIB	Focused Ion Beam
GPa	Giga Pascal
HUT	Helsinki University of Technology
IMCs	Intermetallic Compounds
In	Indium
IPC	Institute for Interconnecting and Packaging Electronic Circuits
JEDEC	Joint Electron Device Engineering Council
K	Kelvin
KJ/mol	Kilo joule per mole
Mn	Manganese
MP	Melting Point
N	Newton
Ni	Nickel
OSP	Organic Solderability Preservative
P	Phosphorus
PA	Power Amplifier
Pb	Lead
PCB	Printed Circuit Board
Pd	Palladium
POP	Package on Package
Ppm	Parts per million
Pt	Platinum
PWB	Printed Wiring Board
Q	Activation energy
QFN	Quad Flat No leads
Sb	Antimony

SEM	Scanning Electronic Microscope
Si	Silicon
SIP	System in Package
Sn	Tin
TEM	Transmission Electronic Microscope
UBM	Under Bump Metallurgy
V	Vanadium
WLCSP	Wafer Level Chip Scale Package
wt. %	Weight percent
Zn	Zinc
Ω	Ohm

1. Introduction

Consumer electronics are becoming increasingly portable with ever increasing functionalities. This is being accomplished through concepts of convergence, integration, and miniaturization. Appliances are becoming smaller, cheaper, lighter, faster and better. Portable electronics in addition are becoming personalized in terms of their design and visual appeal. Attendant with their high functionality, a high level of performance and reliability is expected. They are intended to function under a variety of environmental conditions and mechanical loads. From a user point of view, they need to operate satisfactorily under a multitude of user conditions.

There are several levels of interconnections among the various constituents of the appliance. These include internal connections on the silicon, the silicon to the carrier, carrier to the substrate, interconnections among the various sub-elements and subassemblies. Failure of an appliance is often associated with failure of an interconnection. For example, the functionality of a mobile phone or other portable devices is realized through thousands of solder joints between the silicon device and its substrate, or between the packages or modules and the printed wiring board (PWB) interconnections. The interconnection of the silicon device to the substrate pads is generally either through wire bonding with a gold or copper wire or a flip chip interconnection where the silicon with its I/Os bumped with solder balls are attached to the substrate, with the active face down. This is called first level interconnection. The packages themselves are attached to the PWB using a surface mount assembly process wherein the interconnections between the leaded, leadless or grid-array terminations are made with a suitable solder alloy. Thus, a solder interconnection not only provides the electrical connection but also provides a good mechanical connection for the integrity of the product. An electrical failure may indicate or imply an interconnection failure. A package-to-board interconnection failure may generally involve a solder joint failure. Hence, the performance and reliability of an electronic appliance very much depends on the solder interconnection quality and integrity.

There are different types of packages with different functionalities that are involved in the fabrication of electronic appliances. The packages come in different form factors, and different lead or termination configurations. Some of the lead or termination formats include, J-leads, gull wing leads, area array solder balls, leadless flat land terminations, land grid arrays, etc. Some of the advanced package/modules include: Quad Flat No leads (QFN), Flip Chip Ball Grid Array (FCBGA), Chip Scale Package (CSP), Wafer Level Chip Scale Package (WLCSP), Package on Package (POP), System-in- Package (SIP), stacked die, etc.

The functionality of microelectronics packages or microsystem modules is getting more and more sophisticated. The high functionality and integration also increases the I/Os of some of these packages. The space constraints and miniaturization of these devices lead to finer lead and termination pitches. For instance, the pitch in the current flip-chip technology is 150 μm [1,2]. It will continue to get smaller [3,4] and the smallest flip chip solder bumps reported in the literature so far is 30 μm in diameter [5,6]. Reliability of interconnections with such small solder joints is one of the major concerns for the high density package assemblies. In addition, the implementation of lead (Pb)-free alloys, replacing the traditional Sn/Pb eutectic alloy, has increased the complexity of interconnection metallurgies. Many reliability issues that have hither to not been encountered have now become issues and concerns.

It is important to be cognizant that, even if a single joint of a device fails, the entire product fails. A solder joint involves not only the solder alloy, but also the surface materials of the soldering pads. During bonding process, the molten solder dissolves metals from the soldering pads. During field applications, the solder joints are exposed to high temperatures, resulting in accelerated solid-state interfacial reactions between solder and pads. These will bring changes to the composition and microstructure of the solder joints and, more importantly, the microstructure of the interfaces on the two sides of the joints. It is well known that the properties of an alloy depends not only the alloy composition but also the microstructure. The objective of this dissertation, therefore, is to investigate the reliability of solder interconnections of high density advanced

packages and PWB assemblies from the viewpoint of interconnection material metallurgy under different loading conditions.

The material comprising this dissertation is organized as follows. In Chapter 2 are described the joint reliability challenges from a metallurgical, mechanical, electrical, and environmental perspectives. In Chapter 3 are summarized the effects of microstructure on solder joint mechanical reliability. The design of solder alloys for different applications in electronic assembly and packages is addressed in Chapter 4. This is followed by a description of board level reliability (BLR) test methods in Chapter 5 that were employed in this study. Statistical analysis of test data utilizing Weibull distribution is also discussed. The significant conclusions of this investigation are then summarized.

2. Reliability challenges

In wafer level chip scale packages (WLCSP) or flip chip ball grid array (FCBGA) packages, solder joints are fabricated between two metal systems. On the die side, it is called under bump metallization (UBM) and consists of one or more layers of metals. On the other side, namely, on PWB or BGA substrate, the metal system is usually Cu with protective coatings such as organic solderability preservative (OSP) or Ni/Au plating. **Fig. 2-1** shows a schematic of such a multilayer systems on an FR-4 substrate and semiconductor chip. Reliability of such a joint is directly affected by solder composition, nature and thickness of UBM, pad finish, package size, environment, service conditions, etc. These aspects can be addressed in four convenient categories: 1) metallurgical, 2) mechanical, 3) electrical, and 4) environmental. A brief description of each of these factors is given below.

2.1 Metallurgical reactions

During the reflow process, solder is melted at about 20-25 degrees above its melting temperature. A series of metallurgical events occur in the reflow process. UBM or pad

surface finish material is partially dissolved into the molten solder. One or more intermetallic compounds (IMCs) or phases form at the interface. Spalling of IMC layers may happen, depending on the reflow time and thickness of the surface finishes.

After solidification, the interfacial IMCs may grow thicker, microstructure of the bulk solder may coarsen, and a new IMC layer may form at the interface, depending on the temperature to which the assemblies are exposed. Cross interaction of the metals on the two sides of the joint is another influential factor that could be easily overlooked.

Dissolution of metals: After solidification, diffusion continues in the solid state, but the material transport takes place at a much slower rate. **Fig. 2-2** shows the thermodynamically calculated solubility of metals in eutectic SnPb and SnAg solders. The solubility ranking, namely, the decreasing order of solubility is Au, Ag, Pd, Cu, Ni for SnPb solder and Au, Cu, Pd, Ni for SnAg solder. Higher solubility of a metal results in a greater gradient of its concentration in the molten solder and thus a greater dissolution rate of the metal. It is well known that the dissolution rate of Ni is the slowest in both solders. Because of this, Ni is widely used as a barrier layer between the Cu pad and solder. The solubility of Cu and Ni in lead free solders are known to be much greater than in the eutectic SnPb solder, which results in higher dissolution rates [7].
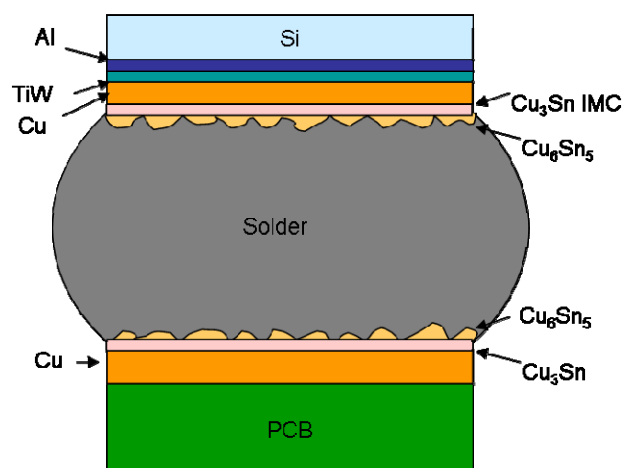
Fig. 2-1 Schematic view of one example multi-layer system of a CSP joint. (Figure not to scale!)
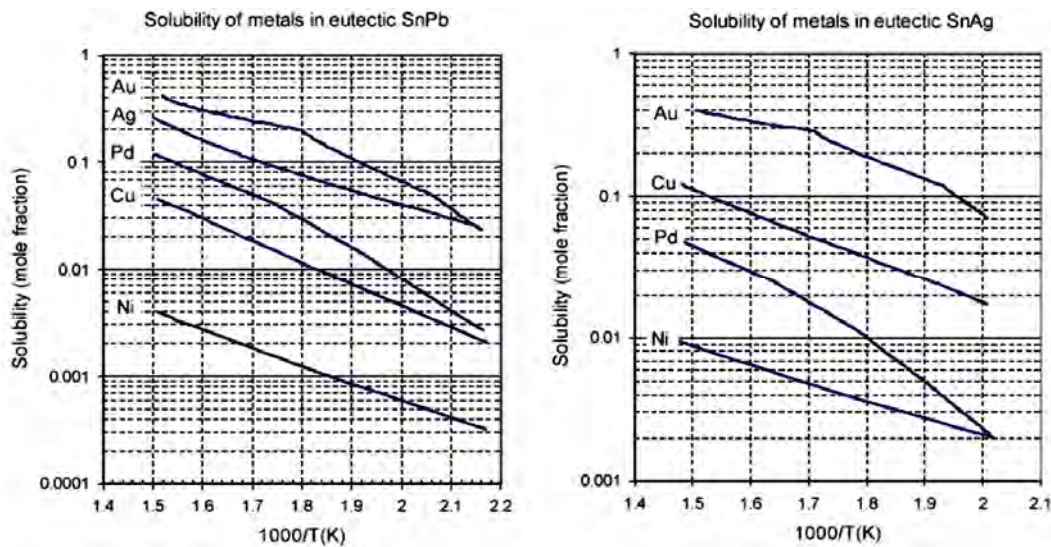
Fig. 2-2 Solubility of Cu & Ni in eutectic Sn-Ag are much greater than in eutectic Sn-Pb solder. This will result in greater dissolution rates [Courtesy by K. Zeng]

Interfacial reactions: During the reflow process, when the concentration of metal exceeds its solubility in the molten solder at the given temperature, intermetallic phases or compounds (IMC) form on the UBM or pad surface. The IMCs are usually those with Sn, such as $AuSn_4$, Cu_6Sn_5, and Ni_3Sn_4.

During reliability tests, such as high temperature storage and thermal cycling, or high temperature field applications, interfacial reactions continue. The IMC layer that is formed by solid state diffusion, or Cu_3Sn in the Cu/SnAgCu joints, continues to grow thicker, whereas the first IMC layer that formed when the solder was in the molten state, or Cu_6Sn_5 in the Cu/SnAgCu joints, is relatively flattened. The inter-diffusion rates of elements within the solder matrix are different. One element may diffuse faster than the other, leaving behind tiny vacancies. **Fig. 2-3** depicts the evolution of micro-voiding in interfacial structures with aging temperature and time on the CSP side [8]. The micro-voiding level increases with temperature and time.

IMC spalling: The interfacial IMC layer may migrate from the interface towards the bulk solder. This is called spalling. This phenomenon has been observed in SnAgCu solder joints on NiAu UBM [9-11]. In this system, after multiple reflows, a two-layer

structure of Ni_3Sn_4 and Cu_6Sn_5 form at the interface as mentioned above. Because of the weak bonding between these two IMCs, Cu_6Sn_5 layer may spall due to its internal compressive stress. See **Fig. 2-4**. If the Ni plating also has compressive stress, the two layers of IMCs can easily separate from each other and cause interfacial failure.
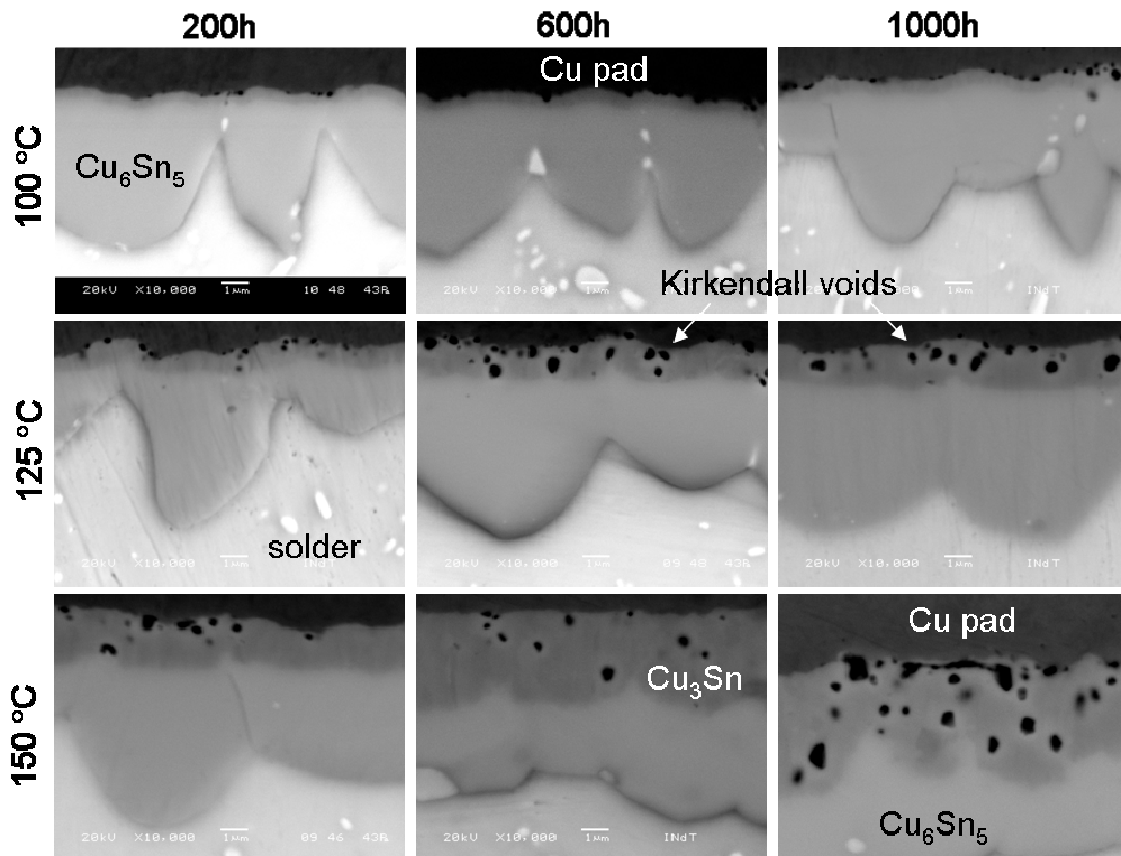
Fig. 2-3 Evolution of interfacial structure with aging temperature and time on CSP side. Aging temperature: Upper row - 100°C, middle row - 125°C, lower row - 150°C.

Cross interactions: Because of the fast migration of some metals into the molten solder, such as Au and Cu, and the small size or volume of solder joints in advanced packages, metallization on one side of the joints can influence the solder reaction on the other side. One example is the flip chip package with Ni(V)/Cu UBM mounted on a Ni(P)/Au plated Cu pad. The size of the joints was 100 μm in diameter. During reflow, Au on the substrate migrated to the die side and enhanced the dissolution of Ni from the UBM system, leading to IMC spalling from UBM much earlier than expected [12].
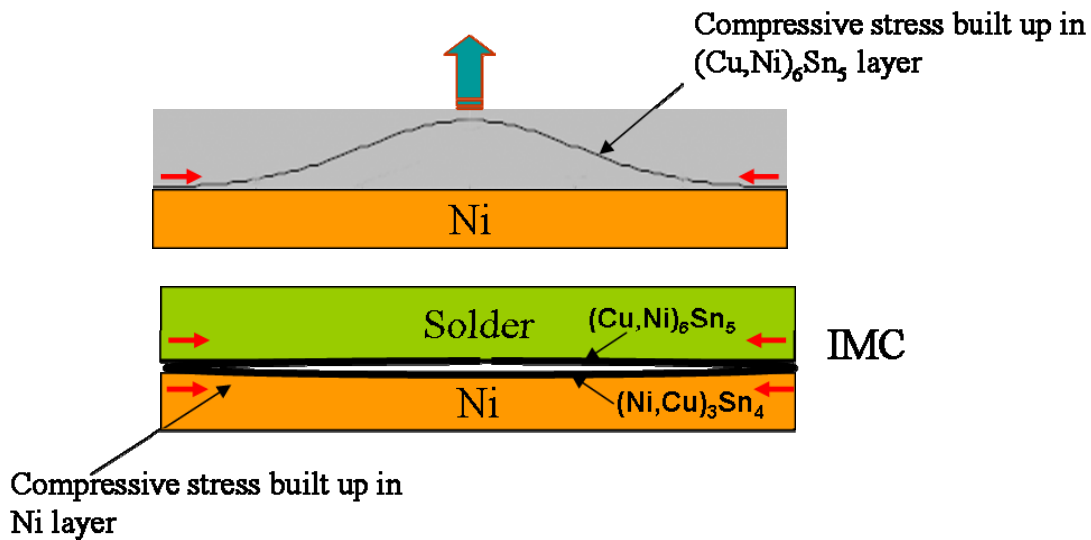
Fig. 2-4 NiAu brittle failure mechanism

2.2 Mechanical

Examples of mechanical loading comprise monotonic or cyclic bending, torque, drop, etc. Mechanical loading during board level reliability test is the major source of stress in solder joints. The stress can be shear, tensile (peel) or a combination. Its distribution across the interconnections depends on the test involved. In a drop test, joints are mainly under tensile stress because of bending of PWB under drop loading [13,14]. In a thermal cycling test, however, due to CTE mismatch between die and BGA substrate or PWB, solder joints are under shear stress (compressive or tensile), depending on their locations. For the joints in the central area of the die, the major component of stress is tensile, but for those in the periphery shear stress is dominant. The farther a joint is located from the die center, the greater the shear stress it has. CTE mismatch $\Delta\mu$ of two different materials is calculated as

$$\Delta\mu = \Delta e \times L \times \Delta T \qquad (1)$$

where

Δe = the difference in CTE between the materials

L = the longest dimension of the component (often the diagonal)

ΔT = the temperature change

Fig. 2-5 shows a schematic illustration of WLCSP and BGA mounted on PWB. The number in each material is its CTE in ppm/°C. According to the above equation, for a 10 mm long package, the CTE mismatch Δ**μ** for WLCSP is 12251.25 ppm.mm.°C, but only 4950 for BGA. Because of this, the solder joints in WLCSP are under much higher stress than in BGA. Obviously, to improve reliability of solder joints in WLCSP is very challenging for reliability engineering of the entire WLCSP.
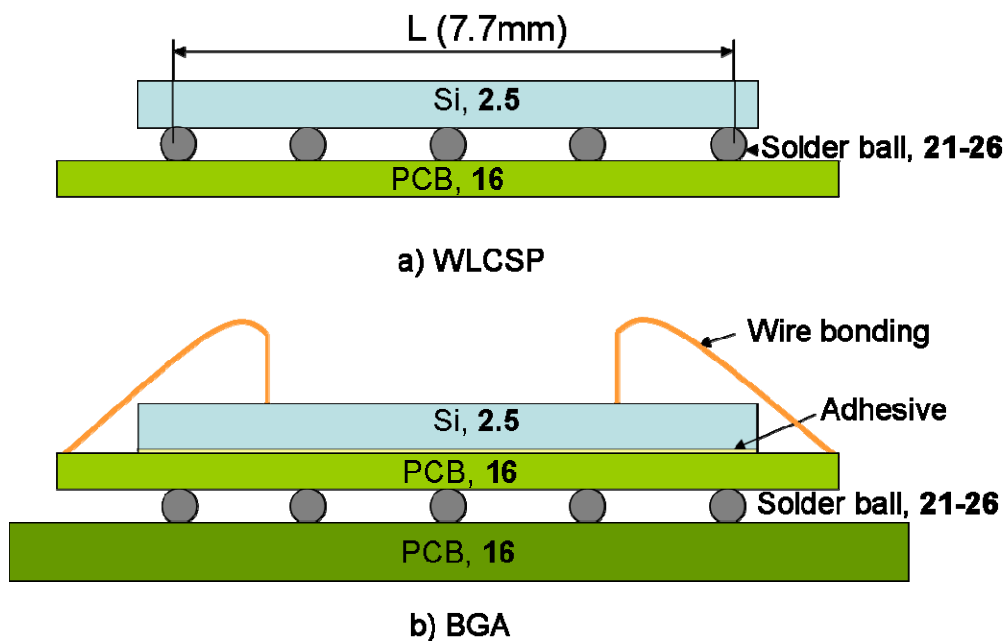
Fig. 2-5 Schematic illustration of WLCSP and BGA mounted on PCB. The number in each material is its CTE in ppm/°C.

2.3 Electrical

Electromigration, electrochemical migration and thermal migration are the failure mechanisms or phenomena that occur when solder joints are under high electrical stress, high humidity and/or high temperature gradient due to joule heating [15,16]. Hu et al. reported that a 14 μm thick Cu stud disappeared from a flip chip solder joint and left a large void there after 95 min at 100°C with a current density of 2.5×10^4 A/cm^2 [17]. Cu atoms were dissolved from the Cu stud, moved into the bulk solder and formed Cu-Sn

IMC on the other side of the solder joint under a driving force of electric current plus joule heating. During current stressing, heat is generated due to joule heating. The joule heating from the silicon die may maintain a huge thermal gradient in the solder joint, causing migration of atoms. Thermal migration has been reported by Ye *et al.* in SnPb solder alloy at a gradient of 1500 °C/cm [16]. Further, if a package or its assembly is not only under high current density but also under high humidity or in the presence of mixed corrosive gases, electrochemical migration can occur. This is especially the case for fine pitch solder joints [18]. Therefore, if a package interconnection is designed to work under a high density of electric current, it should be kept in mind that it may suffer from failures by electromigration, electrochemical migration, or thermal migration.

2.4 Environmental

The environment for solder joints in advanced package interconnections may be harsh. It can be high humidity, too cold or too hot, and even a corrosive environment. If the package-to-board interspaces are not completely filled or has flux residue around the solder joints, the situation becomes even more complex. It has been reported that solder joints failed the temperature humidity and bias test because of the flux residue [18,19]. It is well known that moisture absorption is one of the main contributors to the failure of adhesive joints [20]. Moisture can also contribute to the failure of solder joints because, when electrical current is applied and there is adequate flux residue around the joints, moisture bridges between fine pitch joints, can cause electrical shorts.

Another issue is "tin pest" which is the result of an allotropic transformation of Sn from white β-Sn to grey α-Sn at 13ºC [21,22]. The transformation is very slow at the equilibrium temperature. If the temperature goes to −10ºC or below, the transformation is faster. Since Sn-based Pb-free solders are Sn-rich, the industry is concerned by this phenomenon for products that are to be used outdoor in the cold regions such as the Nordic countries where the temperature in winter can approach −40ºC.

3. Mechanical reliability of solder joints

Mechanical reliability of solder joints is the joint result of the bulk solder and interfaces on two sides. In this chapter, we will discuss the influential factors for mechanical properties of SnAgCu solders, including tin pest, and the interfacial phenomena in SnAgCu solder joints.

3.1 Mechanical properties of SnAgCu solders

It is well known that mechanical properties of metallic materials are very much dependent on the microstructure, composition, and fabrication process. Once the composition of alloy and its process are determined, a specific and characteristic type of microstructure is obtained. As a result, the mechanical properties of the alloy are largely determined by the microstructure. Changes in microstructure in solder joints directly impact their reliability, and thus the operational life of electronic packages. Therefore, reliability engineering of solder joints from a metallurgical perspective is all about how to control the microstructure by designing solder composition, selecting surface materials on both sides, and optimizing the manufacturing process.

3.1.1 Dispersion strengthening effect of IMCs

The eutectic composition of SnAgCu solder is about 3.4Ag and 0.8Cu (wt.%) [23-25]. Because of the low Ag and Cu solubility in solid Sn, most of the Ag and Cu in SnAgCu solder react with Sn to form Ag_3Sn and Cu_6Sn_5 in the matrix of βSn. In the eutectic structure of $Ag_3Sn + Cu_6Sn_5 + \beta Sn$, these two phases are in the form of fine fibers and rods [26-28]. In metallurgical cross sections, they appear as finely dispersed particles (Hereafter, they will be referred as particles instead of fibers or rods). The presence of the fine IMC crystals has both advantages and disadvantages for interconnection reliability. On the one hand, they increase the fatigue resistance of the bulk solder, which is desired for thermal cycling performance of package interconnections. On the other hand, because of their strengthening effect, the SnAgCu solder is much stiffer than

SnPb solder. This renders it more difficult to deform the solder joints. As a result, mechanical stress is not easily relieved or relaxed, resulting in more interfacial failures in drop test [29]. The low drop performance of Pb-free package interconnections has been a hot topic of considerable interest in Pb-free packaging reliability [30-33].

It has been reported in the literature that by cycling, either thermally or mechanically, SnAgCu solder joints develop cracks predominantly along the grain boundaries by grain boundary sliding [34-43]. Therefore, anything that can slow down grain boundary sliding can improve the fatigue resistance of SnAgCu solders. By using TEM (transmission electron microscope), Kerr and Chawla observed that the fine and homogeneous dispersion of Ag_3Sn particles in the eutectic structure pinned the grain boundaries [44]. The Cu_6Sn_5 particles in the eutectic structure have a similar effect, but less significant because usually the Cu_6Sn_5 crystals in the eutectic structure are larger than Ag_3Sn [45]. Therefore, the Ag-containing solders (Sn-Ag and Sn-Ag-Cu) exhibited higher thermal fatigue resistance than the Sn-Cu solders [46]. Performance of SnAgCu solder joints in thermal cycling improves as the Ag content increases, but the Ag content should not exceed 3.0 wt.%. Large plate-like Ag_3Sn crystals grow from the interface when the Ag content is higher than 3 wt.% [47-49]. The Ag_3Sn plates provide easy channels or pathways for crack propagation, degrading the fatigue resistance [12,49,50]. The rank of thermal cycling performance vs Ag content was determined as 2.5>2.0>1.5>1.0>3.0 (wt.% Ag) [51]. This is consistent with findings by Lee and Subramanian that SnAgCu solder joints with 2.5% Ag was better than with 4.0% Ag during thermal cycling between −15 and 150ºC [52].

Under mechanical loading, the finely dispersed Ag_3Sn particles also act as pins to hinder the motion of dislocations in the solder, as confirmed by TEM observations [44]. It is known that the ability of an alloy to deform plastically depends on the ability of dislocations to move within it. According to the Orowan model [53], the yield stress (τ) of an alloy has the following relationship with the dispersed particles that cannot be cut but bypassed by dislocations:

$$\tau \;\propto\; \frac{Gbf^{1/2}}{r}\ln(\frac{2r}{r_0}) \;\approx\; \alpha\, f^{1/2}\, r^{-1} \qquad (2)$$

where G is the shear modulus, b is the Burgers vector, f is the volume fraction and r is the radius of the dispersed particles, and α is a constant for the type of dislocation (0.093 for edge dislocation, 0.14 for screw dislocation). It can be seen from this equation that the more Ag the SnAgCu solder contains, the more difficult it is to deform. Indeed, experimental measurement found that the higher the Ag content in a SnAgCu solder, the higher the elastic modulus and hardness [54]. SnAgCu solder with 1.0 wt.% Ag was able to accommodate more deformation than with 3.8 wt.% Ag before the interfacial strength was reached by a bending test [55]. Consequently, lower Ag solder joints perform better in drop, impact, and high speed bending, shearing, and pulling tests [30-33,55,56].

Therefore, for BGA packages, if a drop test or high speed tests (pull, shear, bending) is the main requirement, a low Ag (<1.2Ag) content is preferred. But if thermal cycling (T/C) is the main requirement, a relatively higher Ag percentage will be better. It should be pointed out that the composition of SnAgCu solder should be selected based on the stress situation in the solder joints, rather than simply based on the test methods. If the dominant component of the stress is tensile, a low Ag solder is preferred to avoid interfacial cracking irrespective of the kind of test the package is undergoing. On the other hand, if shear stress is dominant, a high Ag solder should be used to retard the propagation of fatigue cracks in the bulk solder. The stress situation in a solder joint depends on many factors such as PWB thickness, die size, die thickness, single sided or double sided assembly, test method, and etc. Stress distribution across the whole package interconnections should be modeled before a proper solder composition is selected.

3.1.2 Effect of thermal aging

According to the Orowan model, the strengthening effect of dispersive particles depends on the volume fraction f and the average diameter of the particles r. See **Fig. 3-1.** From this, it is easier to understand the effect of thermal aging on solder joint reliability.

After reflow, phases in the solder joint are not in an equilibrium state because of the cooling rate of the reflow process of BGA packages is high for the small joints. The Sn matrix of the eutectic structure is supersaturated with Ag and Cu in a metastable state at room temperature. Since the solubilities of Cu and Ag in Sn are very low, there is a driving force for the nucleation of Cu_6Sn_5 and Ag_3Sn precipitates. When sufficient thermal energy is put into the system, for instance by aging at 100ºC, the contents of Cu and Ag in the Sn matrix are decreased by precipitation of Ag_3Sn and Cu_6Sn_5. This process requires the atoms to diffuse over short distances, and the thermal activation energy needed is low. The precipitates of Cu_6Sn_5 and Ag_3Sn from a solid solution of Sn are very small and need high magnification TEM to observe. With the help of TEM, it was found that the tiny Cu_6Sn_5 precipitates with grain size around 50 nm are dispersed in the Sn matrix and a lot of dislocations pile-up inside Ag_3Sn particles [57]. More interestingly, Fouassier et al. observed that after annealing at 125ºC for 600 hours, not only Ag_3Sn but also Ag_4Sn formed in the Sn matrix. They were homogeneously distributed inside the eutectic matrix together with Cu_6Sn_5 [58].

Since the precipitation of these compound phases is by solid state diffusion, they are very small and thus have significant strengthening effect. These fine precipitates strengthen the bulk solder by imposing themselves as obstacles to the dislocation glide in the Sn matrix, either by pinning or by differences in Burgers vectors along nearly coherent lattices. As a result, this process helps build up stress in the interfacial region, degrading drop performance, especially at low temperature aging such as 100ºC. After 200 hours of aging at 100ºC, drops to the first failure were decreased from 60 to 30 (**Fig. 3-2**). The drop test samples were CSPs, with Sn3.8Ag0.7Cu solder balls, assembled on

the test boards. The soldering pads on both package side and board side were coated with OSP [8]. The test conditions were described in Section 5.1.
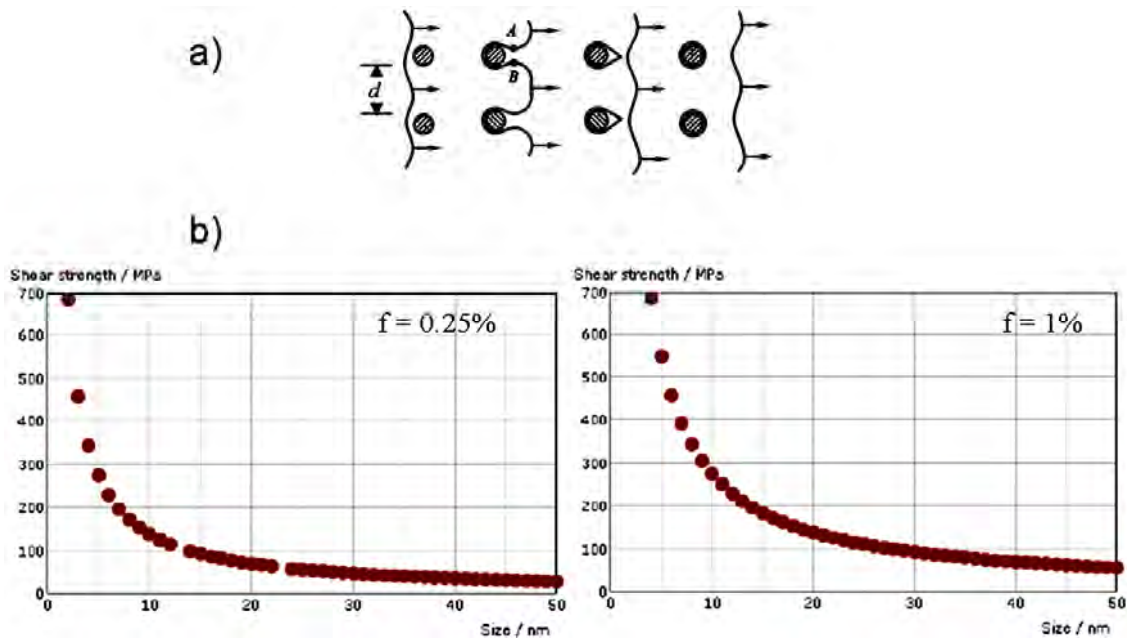
Fig. 3-1 Orowan model of dislocation strengthening. a) Schematic illustration of a dislocation bypassing dispersive particles, where d is the distance between two particles. b) Calculated shear strength as a function of the particles size.

With longer aging times, another change occurs in the microstructure – coarsening of the IMC particles. Driven by the surface energy, the precipitate particulates merge into larger ones. After aging at 100ºC for 14 days the precipitates coarsened significantly, with the Cu_6Sn_5 particles having coarsened more than Ag_3Sn [59]. In addition to the general coarsening of Ag_3Sn particles, aging at 150°C for 24 hours caused the formation of contiguous Ag_3Sn boundaries in the eutectic regions [60]. According to Eq. (2), the larger the dispersive particles, the smaller their strengthening effect. Different from the precipitation, the coarsening process requires the atoms to diffuse over longer distances and thus takes longer time. High temperature can significantly enhance this process. It was recorded that the degrading effect of thermal aging at 100ºC on drop performance of SnAgCu joints faded with aging time after 500 hours (**Fig. 3-3**). In contrast, aging at 125 and 150ºC did not have the degrading effect on drop performance. At these

temperatures, coarsening of Cu_6Sn_5 and Ag_3Sn particles was apparent as shown in **Fig. 3-4**. As expected from the Orowan model, after aging at these temperatures, the solder became softer. The shocking energy by drop tests was absorbed by plastic deformation of the solder ball, resulting in better drop performance (**Fig. 3-2**) [8].
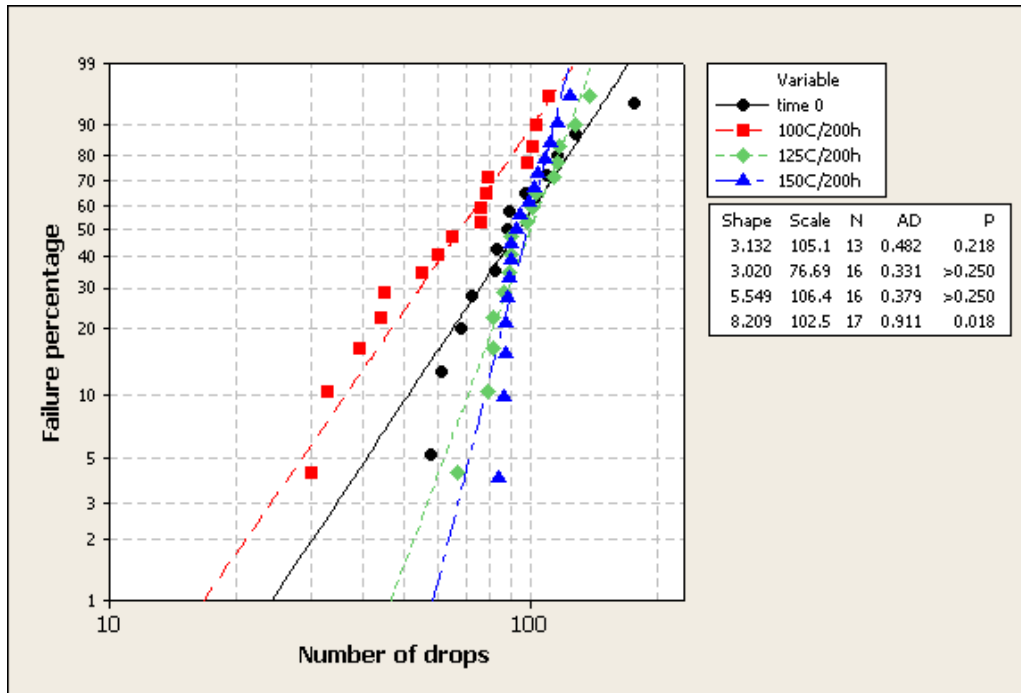
Fig. 3-2 Weibull plotting of drop test data at time 0 and after thermal aging at 100, 125, and 150°C for 200 hours.

Similar results have been reported of the other mechanical properties. After aging at 150°C up to 1000 hours, micro-hardness of Sn-4.0Ag-0.5ACu solder was reduced from 0.27 GPa to 0.12 GPa [61]. Xiao et al. [62] took more measurements in the early stage of aging at 180ºC and found that the thermally aged Sn3.9Ag0.6Cu alloy was initially softened more than after longer time aging. The minimum tensile strength was reached after one day. This softening correlated with the growth of relatively large Sn-rich crystals and with the coarsening of Ag_3Sn particles. When aged at 180ºC beyond one day, the Sn3.9Ag0.6Cu alloy recovered part of its lost strength, but was still weaker than as-reflowed state. The rebounding of tensile strength correlated with the precipitation of Ag_3Sn particles in Sn-rich crystals. It is expected that the strength of the

solder will decrease with aging time again if the aging time is long enough for the precipitation process to be completed.
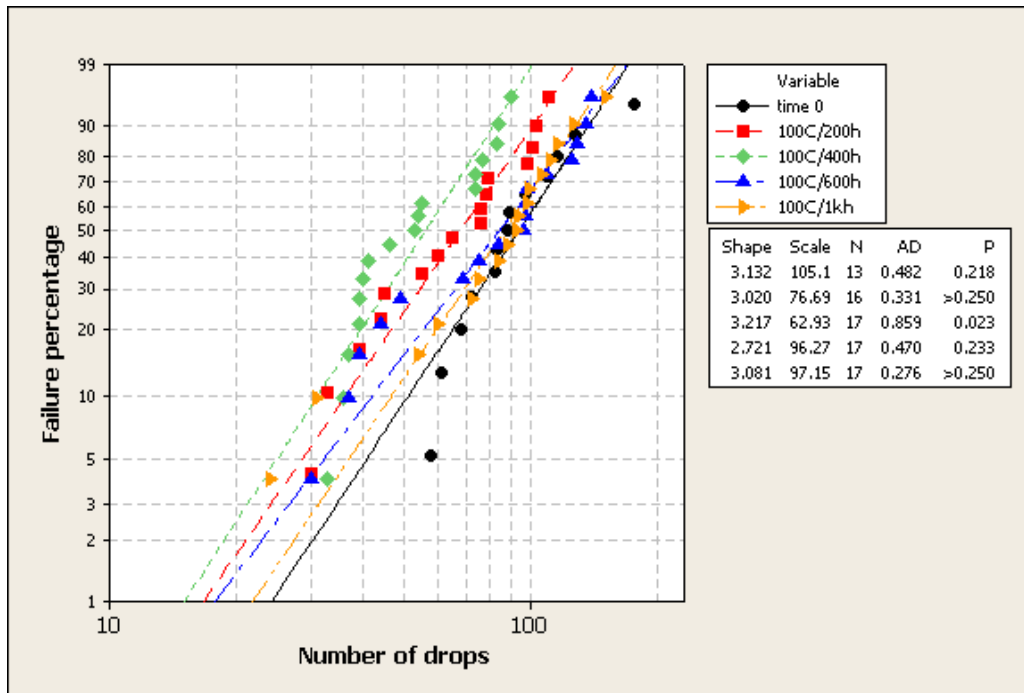
Fig. 3-3 Weibull plots of drop test data at time 0 and after aging at 100°C for 200, 400, 600 and 1,000 h.

Though it is not practical in the industrial production to apply thermal aging to improve drop performance of portable devices, the finding of the effect of thermal aging on SnAgCu solder joint reliability in this investigation still has important practical implications. First, it indicates that the drop performance of Pb-free packages cannot be properly characterized by drop test at room temperature because, during application, the solder joints are exposed to high temperature. The actual drop reliability of the packages may be better or worse than the drop test data demonstrated, depending on the thermal environment in which the solder joints are located. Second, in a mechanical model of Pb-free packages if the effect of the thermal environment on the microstructural evolution of the solder joints is not taken into consideration, any prediction of lifetime of the package from the model will have great deviation from the reality. Therefore, it would be better if the drop test is performed at the maximum working temperature of

the device and the mechanical modeling is based on the data from the high temperature drop test.
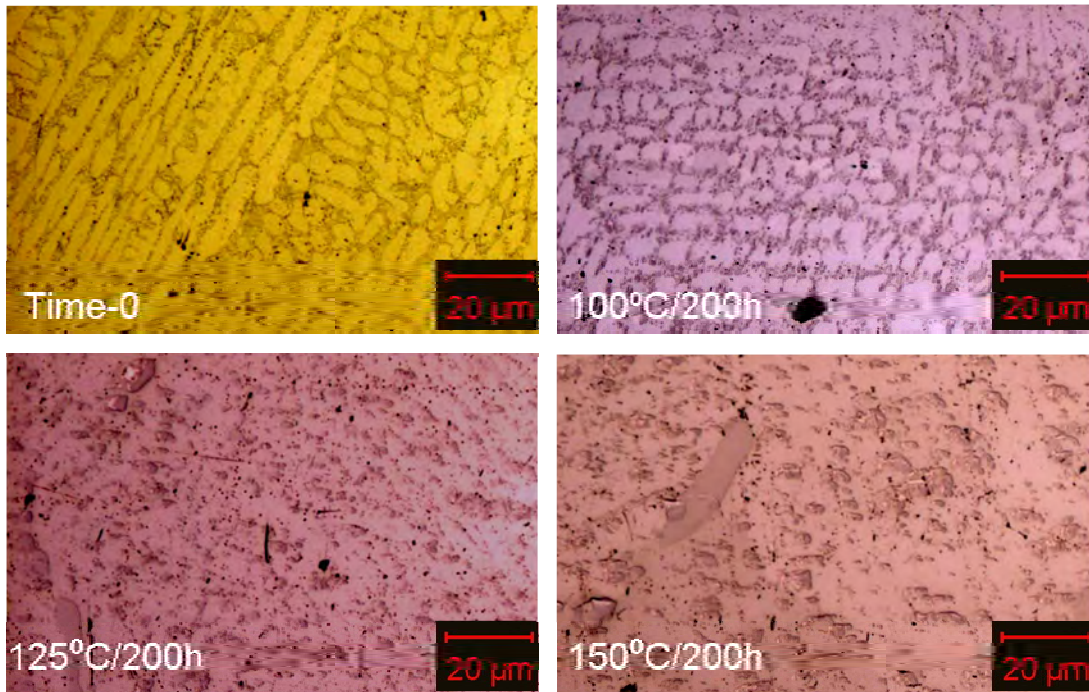
Fig. 3-4 Microstructures of solder joints at time 0 and after thermal aging for 200 hours. After aging at 125 and 150°C, the eutectic structure was significantly coarsened and the dendrite structure disappeared.

3.1.3 Strain rate hardening

The test methods that are widely used to assess solder joint reliability are solder ball pull and shear at component level, and thermal cycling and drop test at board level. During these tests solder deforms, generating dislocations. The dislocations interact with each other and with obstacles which impede their motion through the crystal lattice, resulting in hardening of the bulk solder. This is known as work hardening or strain hardening. On the other hand, since the homologous temperature of Sn at room temperature in Kelvin is $>0.59T_{mp}$, the rate of diffusion of Sn atoms in the lattice becomes appreciable. This allows dislocations to climb over obstacles such as the fine IMC crystals. Then recovery occurs, resulting in the reduction of dislocation density and

work hardening. Recovery is a time-dependant processes because it is determined by the rate of diffusion and the time allowed for diffusion, such as the period of a thermal cycle. The strength at a given strain rate is a balance between recovery and work hardening. The strength, which increases with strain rate, is thus very much a function of strain rate. This phenomenon is known as strain rate hardening.

Strain rate hardening has been observed in both SnPb and Pb-free solders, but the two types of solders have shown different sensitivities to strain rate. SnPb is more sensitive to strain rate than SnAg [63,64]. After work hardening in the very early stage of deformation, SnPb softens with strain at a low strain rate [64-67], but no such behavior of SnAg-based Pb-free solders has been reported [63,64,66-68]. At a high strain rate, SnAg solder gets more work hardening than SnPb [63,66,67]. These differences between SnPb and SnAg-based solders are due to the impeding effect of Ag_3Sn on the motion of dislocations. Ag_3Sn is a complex orthorhombic phase and is not likely to be shearable. Dislocations that encounter these particles will either climb over or bypass the obstacles by the Orowan mechanism. One result of Orowan looping is an increase in the dislocation density and thus more work hardening of SnAg-based solder alloys. Without Ag_3Sn particles, the density of dislocations and substructures (cells and subgrains) in the SnPb alloy is more easily reduced by the thermally activated processes as mentioned above, leading to higher sensitivity to strain rate.

The fact that SnAg-based solders get more work hardening than SnPb at a high strain rate is an important consideration to the manufacturers of portable electronic devices that are usually required to pass a drop test. It is estimated that the strain rate by a drop test is about 10^3 %/sec, much higher than that of thermal cycling tests ($\sim 10^{-3}$ %/sec). The flow stresses of solders are expected to be about 2 to 3 times higher in drop tests than in the thermal cycling test and more concentrated in the corner regions of solder joints [68]. Under the conditions of a drop test, SnAgCu solders will become even stronger than SnPb solder, resulting in a lower performance of package assembly because of the higher rate of interfacial failure. As discussed above, this is because of the presence of Ag_3Sn particles in the SnAgCu solders. To improve drop performance

of Pb-free package interconnections, one of the effective approaches is to decrease the Ag content in the solder joints, as discussed earlier.

Because of the strain rate hardening, the results of ball pull and shear tests are dependant of the test speed. Below a critical speed where the failure mode of solder joints is the fracture of bulk solder, the higher the test speed, the higher the pull or shear force will be [69]. If the test speed is above the critical speed so that interfacial fracture becomes dominant, because of the strain rate hardening, the higher the test speed, the more joints will be broken by interfacial fracture. Therefore, to make the test results comparable, the test speed should be the same. Further, if ball pull or shear is to be used to evaluate the interfacial reliability of solder joints, for example to assess the reliability of different surface finish materials, the test should be performed at a high speed above the critical speed to generate as many interfacial failures as possible so that the bonding strength of interface can be measured. Since the failure mode of a solder joint depends not only on the mechanical properties of solder, but also the pad surface finish and the materials beneath the pad, the critical test speed varies with packages. It should be determined by analyzing the failure modes of solder joints after tests at different speeds [70,71].

The situation in thermal cycling is more complicated. Solder balls get work hardened because of the CTE mismatch between silicon and package substrate or between package substrate and PWB. Concurrently, their mechanical properties are also affected by the exposure to temperatures. Therefore, both ramping rate and dwell time during thermal cycling have significant influences on package interconnection performance. At a higher ramping rate, solder joints are deformed at a higher strain rate and the bulk solder becomes stronger, causing higher stress at the solder/pad interface. This is why packages perform worse in thermal shock test than normal thermal cycling test [72]. The dwell time on package assembly reliability is associated with the results of recovery process. When the temperature increases to above $0.5T_{mp}$, i.e. $-28^{\circ}C$ for eutectic SnAgCu solder, the recovery process, including recrystallization, is activated during testing. The recovery process changes the deformed grains into finer grains that are free

of dislocations and thus reduces the strain hardening. As a result, at a same strain rate, solder that is deformed at higher temperatures will be softer than deformed at lower temperatures [64,65,73,74]. It should be recognized that recovery is a time dependant process because it involves the diffusion of atoms. The shorter the dwell time is at the high temperature extreme, the less the recovery proceeds and thus the less softening the solder can get. Consequently, a package assembly that performs high in the thermal cycling of short dwell time can perform low if the dwell time is increased [72,75,76].

3.1.4 Solder fatigue

Solder fatigue is a typical failure mechanism of solder joints in an electronic assembly by drop or thermal cycling tests. During drop test, the test board, on to which the components are mounted, is subject to repeated bending and thus cyclic stress, but the bending amplitude dampens after each impact [77]. During thermal cycling, due to thermal expansion mismatches between different materials, the solder joints are under cyclic stress. Their fatigue resistance depends on the initial microstructure of the bulk solder as well as the damage evolution during test. While fatigue behavior of SnAgCu solders is largely determined by the Sn-rich phase, because of the low alloying contents, the roles of the IMCs and the phase boundaries should not be neglected.

The eutectic or near-eutectic SnAgCu solders can be solidified into equiaxed or dendritic microstructures, depending on the cooling rate and solidification conditions. The equiaxed microstructures consist of equiaxed Sn-rich grains and dispersive IMC crystals. On the other hand the dendritic microstructures have dendrites of β-Sn surrounded by the fine eutectic structure (**Fig. 3-5**). In the solder joints of electronic assemblies, dendritic microstructure is usually observed. Cyclic deformation tends to concentrate in the dendritic phase, which has been confirmed by the numerous slip bands in the Sn-rich phase [41,46]. Although equiaxed structure of SnAgCu solder is rarely observed in electronic packages after assembly, the dendritic microstructure by solidification can evolve into an equiaxed microstructure upon recrystallization after thermal cycling or a drop test, as clearly shown in Refs. [78-80]. In equiaxed

microstructures, slip bands are also evident in the Sn grains, but grain boundary sliding and microcrack develop early (<5% of the life) in the fatigue life along the grain boundaries [43]. It can be seen from **Fig. 3-6** that cracking of solder joints after the drop test occurred in the recrystallized area near the interface. Korhonen *et al*. [81] confirmed that during thermal cycling the solder joint fatigue process was often initiated with recrystallization of the Sn grains at the stressed area like the neck of the solder joint, resulting in a smaller grain size in the deformed area. Grain boundary sliding in the recrystallized area enhanced nucleation and propagation of cracks, leading to early fatigue failure. Similar observations have also been reported by Mattila *et al*. [82,83].
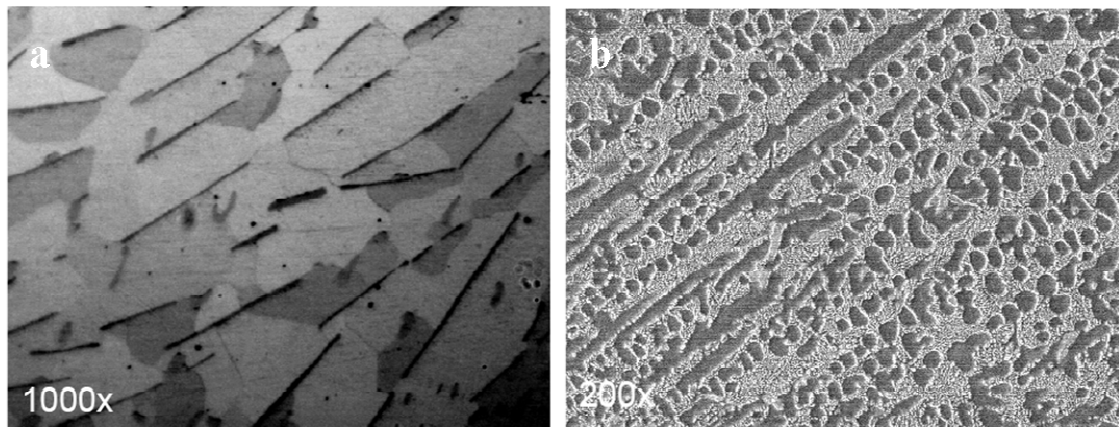
Fig. 3-5 Two kinds of microstructure of SnAgCu solder as solidified: a) equiaxed and b) Dendritic.

In dendritic microstructures, accumulation of cyclic deformation in the β-Sn dendrite leads to fatigue crack initiation along the boundary between the β-Sn dendrite and the eutectic structure or inside the β-Sn dendrite. Cracks can propagate trans-granually through the eutectic structure [84,85]. In equiaxed microstructures, fatigue cracks tend to initiate in the grain boundaries [38,39,43] and prefer high angle grain boundaries [35]. The subsequent crack growth may follow a mixture of trans-granular and inter-granular path [84]. Early in the fatigue life, the individual microcracks are isolated and widely separated. As the density of microcracks increases with continued cycling and approaches the percolation threshold, individual microcracks may coalesce together to form a fatigue crack whose subsequent growth leads to eventual fatigue failure of the

solder. Coalescence of the grain boundary cracks can be blocked by needle-like Ag_3Sn crystals [42]. Hence, in a thermal cycling test SnAgCu solder joints with high Ag content perform better than those with low Ag content [86].
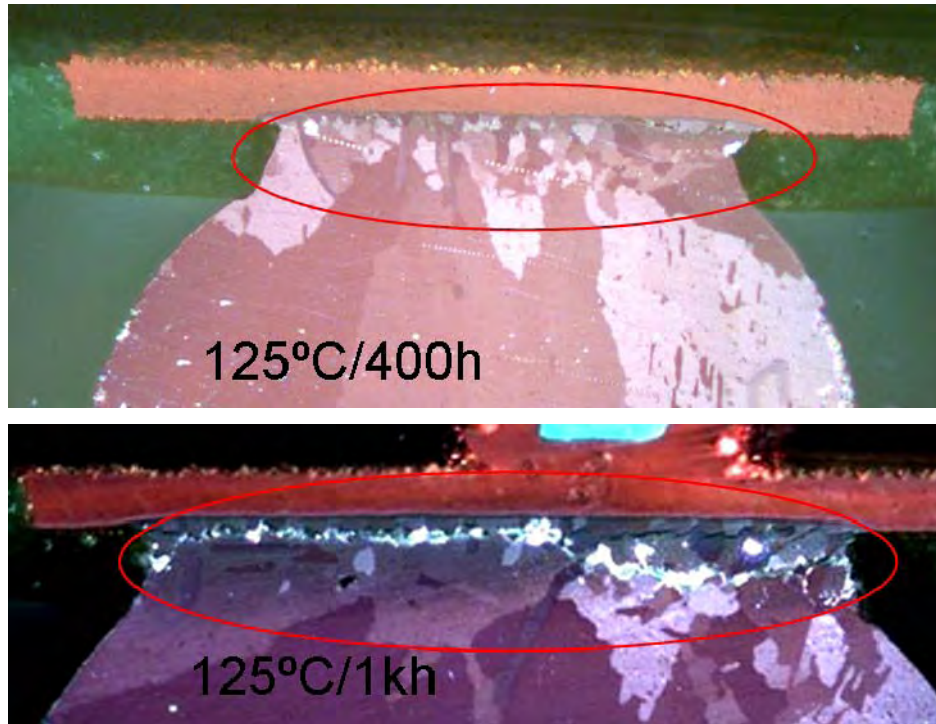
Fig. 3-6 Recrystallized Sn grain boundaries in the neck area and cracks initiated and propagated through the grain boundaries during drop test after thermal aging. Polarized picture.

However, the content of Ag in SnAgCu solder should be lower than the eutectic composition of 3.4 wt.% so that the plate-like primary Ag_3Sn crystals would not precipitate [23]. Because of the smooth surface of Ag_3Sn plates, the interface between solder and Ag_3Sn plates is an easy path for crack propagation (**Fig. 3-7**). The SEM image in **Fig. 3-8** is representative of crack initiation and propagation in SnAgCu solder joints by drop tests. Cracks initiated from the edge and propagated towards the center. Evidence of crack propagation in the ductile solder is clearly seen in the direction indicated by the arrows. It is very likely that there were several initial spots of cracking. In some areas, brittle fracture of IMC crystals also occurred. Exposure of the large

Ag_3Sn crystal in the fracture surface indicates that, if a Ag_3Sn plate is oriented at a small angle to the interface, cracks can initiate at the boundary and easily propagate along the Ag_3Sn/Sn interface, reducing the lifetime of the joint.
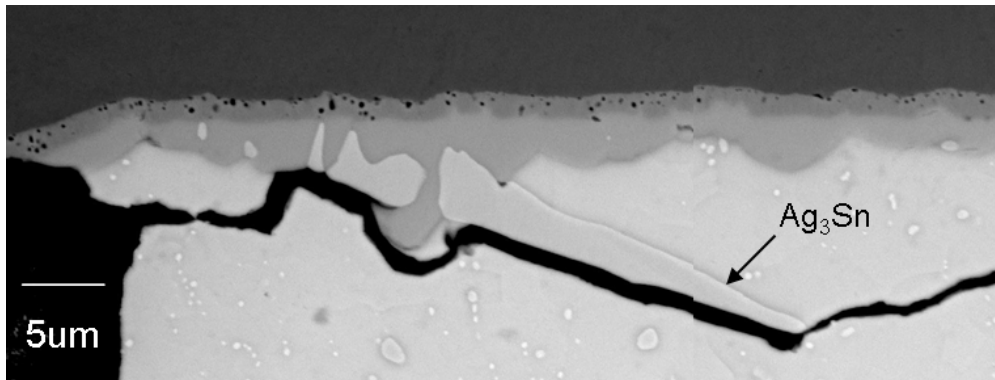
Fig. 3-7 A crack along the interface between Ag_3Sn plate and Sn grain after drop test. The sample was a CSP assembled on a test board and annealed at 150 °C for 200 hours before drop test. Solder ball composition Sn3.8Ag0.7Cu. The sample failed on the component side after 89 drops.
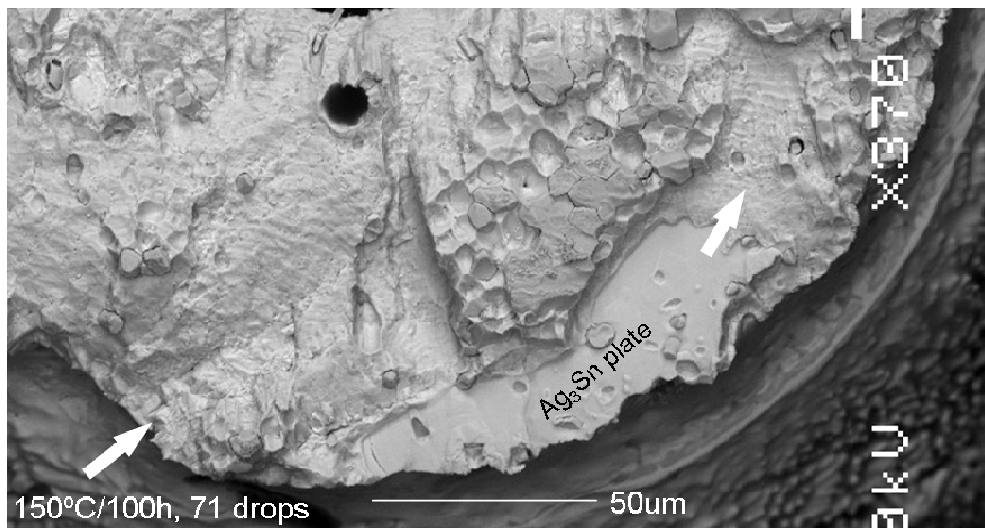
Fig. 3-8 Top view of fractured surface of a solder joint on the ball side after drop test. The sample was a CSP assembled on a test board and annealed at 150 °C for 100 hours before drop test. It failed on the component side after 71 drops. Solder ball composition Sn3.8Ag0.7Cu. Cracks were initiated from the edge and propagated inwards due to cyclic loading by drop impact (cyclic bending).

3.2 Interfacial reaction

In section 3.1, the mechanical properties of SnAgCu solder alloys were discussed. Clearly, the bulk solder plays a critical role in joint reliability. Equally important is the interfacial reaction of solder with the surface materials of bonding pads. During the soldering process, the surface materials of bonding pads are partially dissolved into molten solder resulting in the formation of intermetallic compounds at the interface as well as in the bulk solder. The interfacial bonding strength is greatly affected by the interfacial structure, i.e. the type and morphology of the IMC layers. In addition, the mechanical properties of the bulk solder are modified by the dissolved surface metallurgies. The effects of the UBM of flip chip joints and the pad surface finish of BGA joints on solder joint reliability are discussed. Since the most commonly used surface finish materials for soldering pads are OSP-Cu and Ni/Au plating, we will focus on these two systems.

3.2.1 IMC formation and morphology

OSP-Cu and Cu-Sn IMCs

The organic solderability preservative (OSP) vaporizes at about 150ºC. Therefore, during reflow, the molten solder is in direct contact with the Cu pad. In SnAgCu solder joints with OSP-Cu, Cu_6Sn_5 is the first intermetallic phase to form during soldering. After dipping into pure molten Sn for only one second, the surface of the Cu strip was covered with Cu_6Sn_5 crystals [87]. Formed by reaction of molten solder with Cu, the interfacial Cu_6Sn_5 crystals are hemispherical or rounded (**Fig. 2-3**). If the solder is removed by chemical etching to expose the interfacial Cu_6Sn_5 layer, scallop-like crystals are observed [88]. However, if the Cu content in the molten solder is higher than the eutectic composition of the Sn-Ag-Cu system, which is the case after extended reflow, the primary Cu_6Sn_5 phase will precipitate as rods, needles, or whiskers [28,89]. After Cu_6Sn_5 formation, Cu_3Sn forms by solid state reaction to satisfy the requirements of thermodynamic equilibrium. It is very thin and layer-like after the reflow process, but

it can grow to be easily visible by mean of SEM after high temperature storage. **Fig. 2-3** shows these two IMC layers after annealing at different temperatures. The Cu_6Sn_5 layer has been greatly flattened to reduce the surface energy, but its thickness has not changed significantly. The thickness of Cu_3Sn increased with time and temperature. Kirkendall type of voiding has occurred at the Cu/Cu_3Sn interface and in the Cu_3Sn layer, which will be discussed later.

Ni/Au plating

The dissolution of Au by and the diffusion of Au into the molten solder is very fast [90,91]. In order to avoid the reliability issues caused by the formation of $AuSn_4$ the thickness of Au plating is kept very thin on soldering pads. During reflow of solder joints on Ni/Au plated pads or UBM, Au plating is completely dissolved into the bulk solder. An interfacial reaction occurs between Ni and Sn in the solder. The interfacial reaction in SnAgCu solder joints on Cu is simple as described earlier, but it becomes complex when the UBM or pad finish is a Ni/Au bi-layer. The type of IMCs formed at the interface between Ni and solder depends on the Cu content of the solder. It was thermodynamically estimated that there would be a critical content of Cu in SnAgCu solder joints, below which the interfacial IMC on Ni would be a Ni_3Sn_4-type as observed in SnPb joints, but above that it would be Cu_6Sn_5-type [92]. Experimental studies indicate that if Cu content of solder was less than 0.3 wt.%, the IMC formed on Ni/Au plating was Ni_3Sn_4. When the Cu content was more than 0.6 wt.%, Cu_6Sn_5 formed at the interface. While the Cu content was in the range of 0.3-0.6 wt.%, both kinds of IMCs are formed, but Cu_6Sn_5 did not form as a continuous layer [9-11,93,94].

The observation that the composition of the interfacial IMC in SnAgCu solder joints on Ni matched the formula of Cu_6Sn_5 came as a surprise earlier because it was well known that the interfacial IMC layer in SnPb solder joints was Ni_3Sn_4. Frear *et al*. suggested that the interfacial IMC in the joints of Sn-0.7Cu and Sn-3.8Ag-0.7Cu on Ni UBM was Ni_3Sn_4 [95]. Later, by electron diffraction analysis, Zeng *et al*. confirmed that the interfacial IMC in the Sn3.8Ag0.7Cu solder joints on Ni/Au plating was a hexagonal

phase with the lattice parameters corresponding to Cu_6Sn_5. It was because of the existence of Cu in the solder [92]. Recently, Nogita and Nishimura performed further TEM study of the intermatallic phase in the alloy of Sn-0.7Cu-0.06Ni (wt.%) and it was revealed that the IMC in the alloy was hexagonal Cu_6Sn_5 containing Ni [96].

The interfacial IMCs in SnAgCu solder joints on a Ni/Au plated pad or UBM are actually not pure Ni_3Sn_4 or Cu_6Sn_5. They contain the alloying elements of Cu and Au or Ni and Au, respectively. Thermodynamic calculation of the Sn-Cu-Ni phase diagram predicted that the solubility of Ni in Cu_6Sn_5 could be as high as 20 at.% [92]. This has been widely confirmed in the industry by high temperature storage tests at 150ºC for 1000 hours. Similarly, Ni_3Sn_4 can contain Cu. In electronic packages after assembly, up to 9 at.% Cu was detected in the interfacial Ni_3Sn_4 in solder joints whose solder had only 0.2 wt.% Cu. Though the Au plating is completely dissolved into the bulk solder during reflow, as mentioned above, a small amount of Au is also taken into the interfacial IMC layer. Since Cu, Ni, and Au are all face centered cubic (FCC) metals, they can substitute for each other in the lattice of Cu_6Sn_5 and Ni_3Sn_4. Hence, the formulas of the interfacial IMCs in SnAgCu solder joints on Ni/Au plated pads or UBM can be written as $(Cu,Ni,Au)_6Sn_5$ and $(Ni,Cu,Au)_3Sn_4$.

The morphology of $(Cu,Ni)_6Sn_5$ on Ni is different from that of Cu_6Sn_5 on Cu. In the solder joint of SnAgCu on Cu, the interfacial IMC is Cu_6Sn_5 and the crystals have the shape of scallop [88]. But, the $(Cu,Ni)_6Sn_5$ on Ni is in the form of fine rods or whiskers [97]. The root of the rod contains more Ni than the tip. If exposed to high temperature, more Ni is dissolved into the $(Cu,Ni)_6Sn_5$ layer and more Cu diffuses toward the interface from bulk solder, resulting in the growth of the IMC layer. In addition, coarsening and flattening of the IMC crystals occur. After 1025 thermal cycles between −40 and 125ºC, the whisker-like $(Cu,Ni)_6Sn_5$ crystals have been changed to the equiaxed structure, and a large amount of Cu_6Sn_5 crystals in the bulk solder near the interface has been re-deposited to the interface (**Fig. 3-9**).
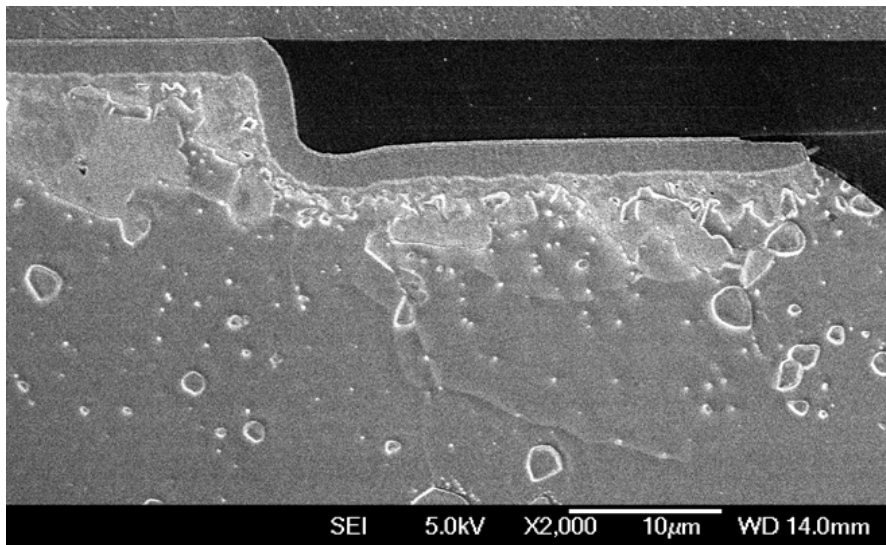
Fig. 3-9 Interfacial structure of Sn-1.2Ag-0.5Cu solder joint on Ni/Au after 1025 thermal cycles between -40 and 125ºC.

According to the phase diagram of the Ni-Cu-Sn system as presented in **Fig. 3-10** [98], a Ni-rich IMC layer should form between $(Cu,Ni)_6Sn_5$ and Ni as required by the local interfacial equilibrium. Indeed, a layer of $(Ni,Cu)_3Sn_4$ formed beneath $(Cu,Ni)_6Sn_5$ after 10 min of soldering at 250ºC [9]. TEM images by Chin *et al*. revealed that the thickness of this layer could even be comparable to that of the $(Cu,Ni)_6Sn_5$ layer [99]. Observation of the dual IMC layer structure in SnAgCu solder joints on Ni/Au plated pads is an important one to the industry from the perspective of solder joint reliability. For long time, the industry has seen high rate of interfacial failure of solder joints in package reliability tests at both component and board levels. **Fig. 3-11** shows such an example after a drop test. It was cracked between Ni_3Sn_4 and $(Cu,Ni)_6Sn_5$. Intel has reported similar observation [33]. In the literature, it has been proposed that it is because the $(Cu,Ni)_6Sn_5$ layer in Pb-free solder joints is more brittle than Ni_3Sn_4 in SnPb solder joints. But, the finding of Ni_3Sn_4 beneath $(Cu,Ni)_6Sn_5$ might have indicated, with more confidence, that the high interfacial failure rate is due to the weak interface between Ni_3Sn_4 beneath $(Cu,Ni)_6Sn_5$. Further investigations are needed to confirm this.
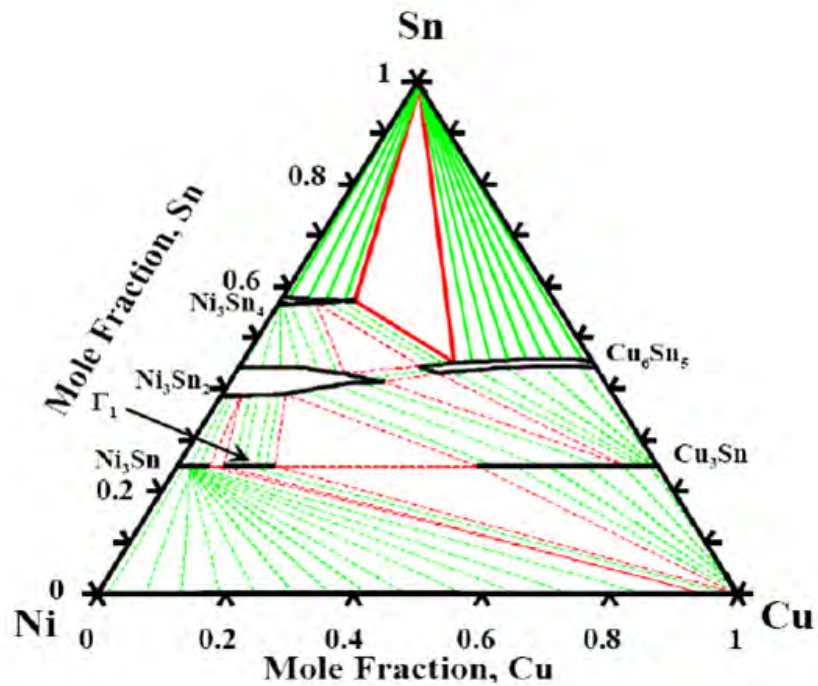
Fig. 3-10 Thermodynamically calculated Ni-Cu-Sn phase diagram at 240ºC. [Courtesy by H. Yu]
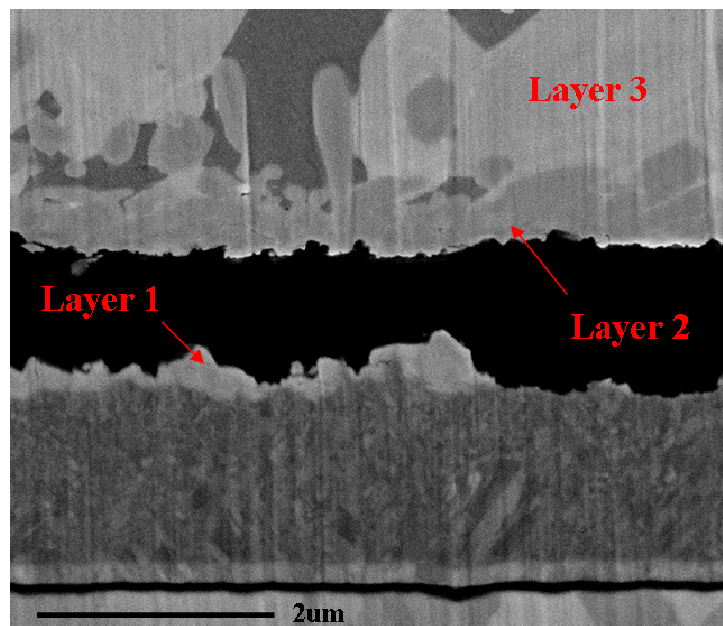
Fig. 3-11 A cracked Sn-1.2Ag-0.5Cu solder joint in Ni/Au plated pad after drop test. There are three layers of IMCs: Layer 1 - Ni_3Sn_4, Layer 2 - $(Cu,Ni)_6Sn_5$, Layer 3 - $(Cu,Ni)_6Sn_5$. Layer 2 contains more Ni than Layer 3.

3.2.2 Micro voiding

Interfacial reaction between solder and pad does not stop after the reflow process. It continues by solid state diffusion, resulting in growth of the interfacial IMC layers and micro voiding at the Cu_3Sn/Cu interface and within the Cu_3Sn layer [100,101]. Based on the measured IMC thickness and position of Kirkendall markers (ThO_2) after annealing at 215°C for 225 hours, the ratio of the volumes, the ratio of intrinsic fluxes of Sn over Cu in the Cu_3Sn layer was found to be [102]:

$$\frac{|J_{Sn}|}{|J_{Cu}|} = 0.9 \qquad (3)$$

This indicates that Cu is the dominant diffusing species and interdiffusion of Cu and Sn through the Cu_3Sn layer is not balanced, as reported earlier by Tu and Thompson [103] and agreed in a recent study of solid state reaction between Cu-Ni alloys and Sn by Vuorinen *et al*. [104]. According to the theory of diffusion, the most prominent diffusion mechanisms are the vacancy mechanism and the direct interstitial mechanism. Since the sizes of both Cu and Sn atoms are large, it is assumed that the interdiffusion of Cu and Sn through the interface proceeds by the vacancy mechanism. By the vacancy mechanism there is a flux of vacancies in the opposite direction of the flux of metal atoms. Because of the unbalanced atomic diffusion of Cu and Sn, atomic-level vacancies left by the migrating Cu atoms on the bare Cu side are not immediately filled by Sn atoms. Coalescence of these vacancies can give rise to the so called Kirkendall voids at $Cu-Cu_3Sn$ interface. However, since the intrinsic flux of Sn is not significantly smaller than that of Cu, as shown in Eq. (3) above, the high level of micro voiding observed in Refs. [8,100,105] was a surprise.

Investigations have been performed to study the root cause for such a fast and high level of voiding process. Yin et al. studied the influence of plating parameters and chemistry on the micro voiding [106-108]. As Cu deposition proceeds, the absorbed species on cathode surface are supposed to be desorbed. If not desorbed, they are incorporated in

the Cu plating. Fragments of the organic additives and their breakdown products are often incorporated in the Cu grains and boundaries. At a high temperature, such as 150ºC for the high temperature storage test of electronic packages, these impurities are vaporized or decomposed, resulting in the formation of voids in grain boundaries of Cu. The voids and some other impurities act as a sink for vacancies generated by interdiffusion of Cu and Sn through the interfacial region, promoting formation of micro-voids. These findings are consistent with the results by other groups. Vuorinen found that the voiding level was different on commercial electrolytic Cu, lab-made electrolytic Cu, and lab-made Cu with brightener addition [27]. After annealing at 125ºC for 500 hours, the Cu plating with brightener showed the highest level of voiding but the commercial electrolytic Cu had the lowest level. Yu and Kim found that additions of SPS (bis-sodium sulfopropyldisulfide, $C_6H_{12}O_6S_4Na_2$) to the Cu electroplating bath strongly affected the characteristics of micro- void formation in Sn3.5Ag solder joints on Cu plated pads after baking [109,110]. Without SPS in the plating bath, voids were observed only in the Cu_3Sn layer of solder joints. In great contrast, with SPS added to the plating bath, voids formed not only in the Cu_3Sn layer but also at the interface between Cu_3Sn and Cu pad. More importantly is that the density of void distribution at the interface was so high that they formed a continuous crack-like defect along the interface. Auger analysis detected sulphur in the cracked interface, which suggests that sulphur from SPS had segregated to the Cu/Cu_3Sn interface and void surfaces.

In a production plating bath, there are many additives. The balance of these additives is affected by more factors than in a laboratory bath, for example, leaching from photo resist, contamination from solder mask, and products of additive breakdown during bath idle time. Though only one additive of SPS has been found so far to be responsible for micro voiding in solder/Cu joints, some other additive may play a similar role in the phenomenon of interfacial voiding if the balance among the additives is broken. It can be concluded that the Kirkendall type effect is not the major contributor to the micro-voiding along the interface between solder and Cu pad, but impurities entrapped in the Cu plating are.

3.2.3 IMC growth in solid state

After the Cu atoms arrive at the interface of Cu_3Sn/Cu_6Sn_5 by diffusion through the grain boundaries of the Cu_3Sn layer, Cu_6Sn_5 is converted to Cu_3Sn at the interface, resulting in the growth of Cu_3Sn towards Cu_6Sn_5. Because of this, the amount of Cu atoms that can further diffuse into the interface of Cu_6Sn_5/solder is greatly reduced. The growth of Cu_6Sn_5 on the solder side mainly depends on the availability of Cu atoms in the solder. Since most of the Cu atoms in the bulk solder have been consumed to form Cu_6Sn_5 particles in the eutectic structure, the amount of free Cu atoms that can diffuse to the solder/Cu_6Sn_5 interface is very limited. Therefore, during thermal aging, the Cu_3Sn layer expands on both sides, with the Cu/Cu_3Sn interface shifting towards Cu pad and the Cu_3Sn/Cu_6Sn_5 interface towards the Cu_6Sn_5.

Generally, the growth kinetic parameters of an IMC layer can be determined by plotting its measured thickness as a function of the exposure time at given temperatures. For the growth of the IMC layer, its thickness as a function of the time can be expressed as

$$Y = Y_0 + \sqrt{Dt} \quad (4)$$

where Y is the IMC layer thickness at time t, Y_0 is the initial IMC layer thickness after soldering, and D is the diffusion coefficient as a function of temperature, which is defined by the Arrhenius equation:

$$D = D_0 \cdot e^{\left(\frac{-Q}{RT}\right)} \quad (5)$$

where D_0 is the diffusion constant, Q is the activation energy for the growth of the interfacial IMC layer, T is the temperature in Kelvins (K), and R is the gas constant, 8.314 J/mol-K.

From the measured thickness data, D can be determined for each experimental temperature. Using Eq. (5), the activation energy Q can be determined from the slope of the straight line obtained by plotting Ln(D) against 1/T:

$$Ln(D) = Ln(D_0) - \left(\frac{Q}{R}\right) \cdot \left(\frac{1}{T}\right) \quad (6)$$

This approach was taken to study the growth kinetics of Cu_3Sn and Cu_6Sn_5 in Sn3.8Ag0.7Cu solder joints in a PWB assembly after thermally aged at 100, 125, and 150 °C for up to 1000 hours. The surface finish of the soldering pads on both component side and PWB side was OSP-Cu. The size of the solder balls was 250 μm in diameter. It was found that the Cu_3Sn thickness significantly increased with aging time at 125 and 150°C, but changed only a little at 100°C. However, the thickness of Cu_6Sn_5 increased only 0.2-0.3um after 1000 hours at 125 and 150°C. Obviously, the increase of total IMC thickness is mainly due to the growth of Cu_3Sn rather than Cu_6Sn_5. At time-0, Cu_6Sn_5 was about 0.5 µm thicker on the component side than PWB side because of the one more reflow the interface on the component side had undergone in the component manufacturing. Except for this, everything was similar on both component and PWB sides: a very similar and clear trend of Cu_3Sn growth with aging time, and very similar Cu_3Sn thickness as reported in Publication II of this dissertation.

3.3 Sn Pest of Pb-free solders

Most of the Pb-free solders that are now widely used for electronic manufacturing are Sn-based, for example, the eutectic Sn-Ag, Sn-Cu, and Sn-Ag-Cu alloys whose contents of Sn are 96.5, 99.3, and 95.8 wt.%, respectively. Concern of Sn pest emerges for the reliability of electronic devices that are to be used in cold regions such as the Nordic countries.

Pure Sn has an allotropic transformation at 13°C, i.e. from white β-Sn to grey α-Sn. White Sn has body centered tetragonal (bct) structure and its density is 7.29g/cm^3. Grey

Sn has diamond structure and its density is 5.77g/cm^3. The transformation is accompanied by a volume increase of 27%. For a cubic unit of material to do that, if it expands in x, y, and z directions at a same rate, its dimension needs to increase by 8.3%. Obviously, in order for the transformation to proceed, a softer matrix of β-Sn is preferred. Otherwise, it can occur only in the free surface [21,22]. Although the transformation is sluggish, it is promoted at lower temperatures. When this occurs, warts and surface cracking are observed. Eventually, the bulk Sn will disintegrate into powders. This is known as tin pest. If the Sn pest happens to the solder joints in electronic package interconnections, obviously it would cause the device to fail.

Four solders Sn-0.7Cu, Sn-3.4Ag-0.8Cu, Sn-3.5Ag and Sn-36Pb-2Ag have been compared with pure Sn at low temperatures for tin pest. The samples were stored at -196 ^{o}C for 50 hours, -40 ^{o}C for 4 years, and finally -17 ^{o}C for 1.5 years. Sn pest occurred in pure Sn plate only, not in any of the solder alloys (**Fig. 3-12**). Tin pest is less likely to cause failure of Pb-free solder joints in electronic devices, but pure tin may [111].

Fig. 3-12 Sn pest in pure Sn plate after 50 hours at -196ºC plus 4 years at –40ºC and plus 1.5 years at –17ºC.

The reason for the effect of alloy elements on the transformation of white β-Sn to grey α-Sn have been discussed from a theoretical basis [21]. Lead was very effective at inhibiting the transformation [112]. Thus, there has been no concern of Sn pest for SnPb soldering. Silver is also known to retard the transformation [113,114]. Though Sn pest was found in cast Sn-0.5Cu solder [115] and Sn-0.8Cu alloy that was melted in graphite crucible [116], it was not observed in our experiments with rolled Sn-0.7Cu alloy foil [111]. Even more interesting, after 7 years of storage at −18 ^{o}C, two samples from the investigation of Ref. [115] with the same nominal composition of Sn-0.5Cu showed totally different results: One was unaffected by this exposure, but the other one had completely transformed into brittle α-Sn [117]. Compositional analysis revealed statistically significant differences in the concentrations of 10 trace elements between the two samples, with the higher always associated with the untransformed sample. The reason for different levels of trace elements in the samples was that the starting materials used for their synthesis were taken from different lots of the same supplier. It was concluded that elements that were soluble in solid Sn suppressed the formation of tin pest.

Therefore, while the effect of alloying element Cu on tin pest is not clear yet and further investigation is needed before a definitive conclusion can be reached, it is generally accepted that any factor that strengthens the tin matrix can increase the resistance to tin pest. The influential factors are solder element, composition, and temperature. A possible explanation is that these elements decorate dislocations and other defects within the alloy matrix, thereby impeding the transformation by inhibiting stress relaxation ahead of the expanding α-Sn [118].

4. Design of Pb-free solder alloys

In this chapter, we will first review different Pb-free solders to see why Sn-Ag-Cu was selected for this study. Then we will summarize how the eutectic composition of the Sn-Ag-Cu alloy was determined and how to use this composition as a reference in selecting Sn-Ag-Cu solder for an electronic package.

4.1 Alloy design considerations

When developing new lead-free solder materials to replace Pb containing solder, it is necessary to first check if it would meet, at least in principle, all the following basic requirements:

- melting temperature or temperature range (and undercooling)
- solderability, especially wettability
- electrical and thermal (conductivity and heat capacity) properties
- thermal expansion coefficient
- mechanical strength and ductility
- creep resistance
- thermal-fatigue resistance
- corrosion resistance
- manufacturability
- availability of alloying elements
- joint stress situation
- compatibility with surface metallurgies

Until now there are no known lead-free solder alloys that meet all these requirements in such an optimal manner as the eutectic or near-eutectic Sn-Pb alloys do. In addition, the choice of a flux, assembly method, solder composition and PWB thickness can influence the properties and performance of the interconnections, greatly complicating matters. Hence, the development of a lead-free solder that has all the desirable properties and allows robust assembling is really a challenging task, the solution of which also demands a systematic study of the processing parameters for defining acceptable process windows for high yields and reliability.

The eutectic 96.5Sn-3.5Ag solder alloy has been used for years in certain electronic applications. A lot of tests have already been completed [119-128]. The conclusion was

that the eutectic Sn-Ag alloy provided acceptable properties. The electrical conductivity, surface tension, thermal conductivity, and coefficient of thermal expansion of Sn-Ag solder were all claimed as comparable with those of the Sn-Pb solder (see **Table 4-1**). The most obvious limitation of 96.5Sn-3.5Ag solder is its melting temperature (221°C), which is 38°C higher than that of the eutectic Sn-Pb solder (183°C), and hence increases demands for heat resistance of components, especially some temperature-sensitive components. However, by adding small amount of a third element such as Cu, Bi, In or Zn, the melting point can be lowered to be 210ºC for Sn-Ag-(In or Bi) and 217ºC for Sn-Ag-(Cu or Zn). Their mechanical, physical, chemical properties are also changed. The characteristics of the four lead-free solder systems, in comparison with the Sn-Pb solder, are summarized in **Table 4-2**. From the literature data, the following conclusions can be drawn:

Table 4-1 Properties of the eutectic Sn-Ag solder compared with the eutectic Sn-Pb solder

Alloy composition	Melting point (ºC)	Density (kg/m^3)	CTE (ppm/ºC)	Electrical conductivity (% IACS)	Electrical resistivity (µΩcm)	Surface tension (N/m)	Thermal conductivity (W/[mk])
63Sn-37Pb	183	8400	21.4/25	11.5	14.99	0.49	57.9/32.6 °C
96.5Sn-3.5Ag	221	7290	22/20	14	12.31	0.48	55.3/23.9 °C

Indium seems to be the most effective element for reducing the melting point of Sn-3.5Ag. It also has exceptional attributes of physical and wetting properties [122,125,129-131]. However, indium is not abundant in nature and is too expensive to be considered for broad application. For these reasons, alloys containing indium is excluded from further considerations. Indium alloys may be perfect candidates for special applications, but are not appropriate for high volume consumer electronics.

Zinc is inexpensive, readily available, and extremely effective in reducing the melting point in tin alloys. SnAgZn eutectic point is 198ºC. The challenges associated with zinc are related to its rapid reaction with oxygen. It quickly forms a stable oxide. The effect of this reactivity is excessive drossing during soldering and, more problematically, very

poor wetting due to the stable oxide formation [132-135]. Perhaps these technical problems can be overcome with the use special flux formulations. However, at the current time, a workable system with zinc has not been demonstrated. For these reasons, zinc alloys are excluded from our further consideration.

Table 4-2 Material characteristics of the Sn-Ag based ternary solder systems in comparison with Sn-Pb solder.

Solder systems	Sn-Ag-Cu	Sn-Ag-Bi	Sn-Ag-In	Sn-Ag-Zn
Manufacturability	Good	Good	Good	Unknown
Thermal expansion coeff.	Comparable	Comparable	Comparable	Unknown
Wettability	Comparable	Better	Worse	Unknown
Pasty range	Comparable[1]	Comparable	Worse	Comparable
Drossing	Comparable	Comparable	Comparable	Worse
Reliability	Good	Good	Good	Good
Mechanical shock	Good[1]	Comparable	See note 2	Better
Vibration	Good[1]	Comparable[1]	Worse	See note 2
Thermomechanical fatigue	comparable	Better	Better	Better
Creep	See note 3	Good	Unknown	Comparable
Corrosion	Good[1]	Worse	Comparable	Good
Ductility	Good[1]	Comparable	Comparable	Good
Strength	Good	Good	Bad	Good
To human health	Moderate	Moderate	Low	Moderate
Availability	Acceptable	Acceptable	Unacceptable	Acceptable

1. Composition dependent.
2. Mechanical reliability is superior to Sn-Pb at high shear stresses, but inferior at low shear stresses [122, 123].
3. Sn-Ag-Cu alloy is fairly resistant to corrosion [136], but the alloy composition was not given.

Bismuth is effective in reducing the solidus temperature of tin alloys, but is not as effective in reducing the liquidus temperature, which results in a broader mushy or freezing range. Bismuth also demonstrates very good wetting properties and good physical properties [23,122,123,125,129-131,136-138]. However, the availability of Bi could be limited by restrictions on lead because, at this time, the primary source of bismuth is a by-product of lead refining. By restricting the use of lead, much less bismuth will be available. Bismuth reserves that are directly mined are available, but the cost can be prohibitive. For these reasons, bismuth can only be considered as a minor additive in Sn-Ag based solders.

Therefore, only the Sn-Ag-Cu ternary system is left as a candidate. Compared to the Sn-Ag-Bi system, Sn-Ag-Cu eutectic has more benefits because at the same superheating above the solidus temperature, Sn-Ag-Cu eutectic has lower viscosity and better fluidity. From metallurgical point of view Sn-Ag-Cu eutectic solder alloy is also a promising candidate. Its microstructure presents a fine equiaxed homogeneous grain structure. Its joint reliability with different surface finishes such as Ni/Au and OSPs (Organic Solderability Preservatives) are compatible if Cu composition is appropriately selected [27,139].

4.2 Sn-Ag-Cu solders

Sn-Ag-Cu alloy wets and forms good quality of joints with copper. It is a promising solder for replacing the conventional Sn-Pb eutectic solder in avionics and automotive applications where the solder joints are subjected to numerous thermal cycles and mechanical vibrations, and are expected to sustain operational temperatures up to 150°C [140,141]. Its thermomechanical property is even better than those of the conventional Sn-Pb solders [142]. Since eutectic solders possess overall better mechanical properties, efforts were expended to determine the eutectic composition of the Sn-Ag-Cu system in the 90s. The eutectic compositions studied by some institutions are listed in **Table 4-3**.

Table 4-3 Sn-Ag-Cu solder eutectic compositions

Investigator	Composition (wt. %)	Ref.
Japan	Sn-3.5Ag-0.7Cu	121
Alpha-Metals	Sn-4.0Ag-0.5Cu	142
Multicore	Sn-3.8Ag-0.7Cu	136
Heraeus	Sn-3.2Ag-0.5Cu	135
Northwestern, USA	Sn-3.5Ag-0.9Cu	139
Ames Labrotary, USA	Sn-4.7Ag-1.7Cu	139
HUT, Finland	Sn-3.4Ag-0.8Cu	23

An alloy with the eutectic composition starts to melt at the eutectic temperature and becomes fully molten or solidified at the same temperature. Its microstructure consists of only fine eutectic structures because no primary or secondary phases can precipitate during solidification. Any deviation from the eutectic composition will result in an increase in the liquidus temperature and appearance of primary and/or secondary phases. If a non-eutectic solder is taken as eutectic, the selected soldering temperature may not be high enough to fully melt it. The un-melted crystals float in the molten solder and will decrease the wettability. Besides, if a solder alloy contains a primary phase that is harmful to the mechanical properties of the bulk materials, the mechanical properties of the solder joint and its reliability will be degraded. Therefore, the importance of determination of the eutectic composition of the Sn-Ag-Cu solder alloy is that it provides a reference composition for solder design. If the effects of the three primary phases, namely, solid solution (Sn), intermetallic compounds Ag_3Sn and Cu_6Sn_5, are clear on the mechanical behavior of the bulk alloy and the interfacial region, and specific requirements have been defined for soldering process and solder joint reliability, it will be possible to quickly determine the proper composition of the solder alloy.

4.2.1 Determination of eutectic composition

In **Table 4-3** are listed some eutectic compositions by several investigators. **Fig. 4-1** shows the locations of the eutectic composition listed in **Table 4-3**. It is generally accepted that the eutectic temperature is 217°C, but the eutectic composition is still in question. Richards [143] proposed that the alloy with Sn-4Ag-0.5Cu (wt.%) would become the most widely used because this particular composition was suggested as the ternary eutectic by Gebhardt and Petzow fifty years ago [144]. By quenching alloy samples into ice water, Ames Laboratory got a completely eutectic microstructure in the alloy of Sn-4.7Ag-1.7Cu (wt.%) and thus this composition was reported as the eutectic composition [140,141]. However, we found that, when a sample of this composition of Sn-Ag-Cu alloy in a Pyrex tube was cooled in vacuum at a rate of about 0.1°C/s (see **Fig. 4-2**), primary Cu_6Sn_5 formed (**Fig. 4-3a and c).** The reaction is L→Cu_6Sn_5 at point A in **Fig. 4-1**. As the alloy was cooled down from point A to B, secondary Ag_3Sn and

ternary eutectic structures formed (**Fig. 4-3b**). The reaction at point B is $L \rightarrow Cu_6Sn_5 + Ag_3Sn$ and at eutectic point E is $L \rightarrow Sn + Cu_6Sn_5 + Ag_3Sn$. Ag_3Sn and Cu_6Sn_5 were recognized in the fine ternary eutectic structure (**Fig. 4-3**). The different microstructures of the same composition of alloys observed are due to the different cooling rates. By quenching into ice water (cooling rate is > 1°C/s) [141], the sample was quickly cooled down below the eutectic temperature and the precipitation of Cu_6Sn_5 and Ag_3Sn from the liquid phase was kinetically suppressed.
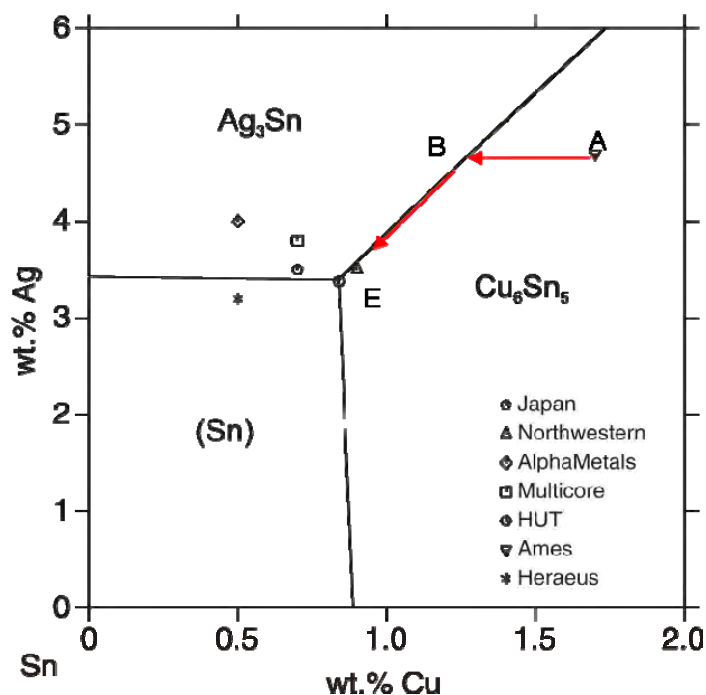
Fig. 4-1 Modified Sn-corner of the liquidus surface projections of the Sn-Ag-Cu system in accordance with HUT experimental results [23]. The "eutectic" data in the literature in Table 4-3 are plotted for comparison. Arrows from A through B to E are solidification path of Ames alloy imposed on the calculated Sn-corner of the liquidus surfaces surface projection of the Sn-Ag-Cu phase diagram

An effective approach for determining the eutectic composition of an alloy system is to combine experimental study with thermodynamic calculations. In our investigation, by extrapolation from the binary thermodynamic data, the eutectic point of the Sn-Ag-Cu solder alloy was estimated at 0.69Cu, 3.3Ag (wt.%), and 218°C. The estimated eutectic

temperature was very close to the experimental one, 216.8 °C, which was measured with DTA at a heating rate of 5°C/min [141]. Therefore, it was believed that the true eutectic composition of the Sn-Ag-Cu solder alloy was not far away from this estimated composition. Then eight compositions of alloys were selected around the estimated eutectic point to experimentally check the microstructures **(Table 4-4)**. The alloy with a composition of Sn-4.7Ag-1.7Cu (Ames alloy) was taken as a reference. The alloys samples were made from pure (>99.99%) commercial metals. They were sealed in vacuum Pyrex tubes and melted in a muffle furnace. In order for Cu and Ag to be completely dissolved into molten Sn, the alloys were held at 315°C for 45 min. After that, they were taken out and shaken to mix the metals. Then they were held at 270°C for 15 mins. In order to let the primary phases precipitate, alloys were cooled within the furnace with the furnace door open so that the cooling rate is about 0.1°C/s (**Fig. 4-2).** It was found that the sample of Sn-3.4Ag-0.8Cu (wt.%) was full of ternary eutectic microstructure without primary and secondary IMCs (**Fig. 4-4**). Though the real equilibrium state might have never been reached by usual laboratory experiments, it was believed that under the experimental conditions described above the alloy samples were close to the equilibrium state. Therefore, we suggest that Sn-3.4Ag-0.8Cu is close to the eutectic point as plotted in **Fig. 4-1** [23].
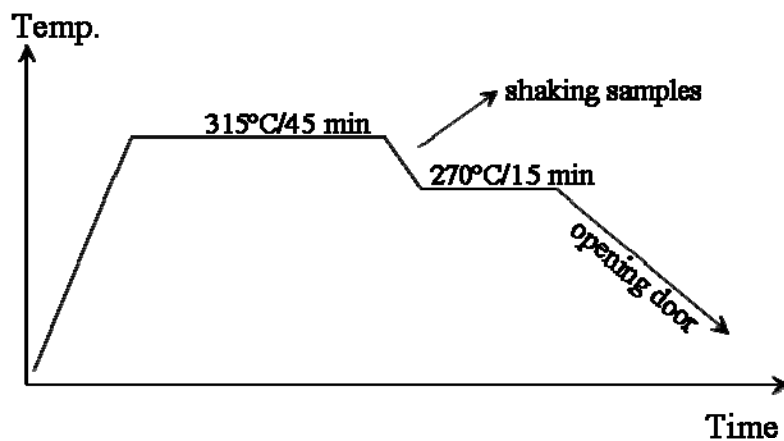
Fig. 4-2 Melting and solidification process of the alloys in six alloys and Ames alloy, cooling rate 0.1°C/s.

Table 4-4 Compositions of Sn-Ag-Cu alloys investigated in this work

No.	Composition in wt. %
1	95.33Sn-4.04Ag-0.63Cu
2	96.04Sn-3.27Ag-0.69Cu
3	96.74Sn-2.75Ag-0.52Cu
4	95.84Sn-3.22Ag-0.94Cu
5	95.46Sn-3.68Ag-0.87Cu
6	94.50Sn-4.27Ag-1.23Cu
7	95.80Sn-3.40Ag-0.80Cu
8	93.60Sn-4.70Ag-1.70Cu

Fig. 4-3a Cu mapping revealed the primary phase Cu_6Sn_5 in Ames alloy (Sn-4.7Ag-1.7Cu).
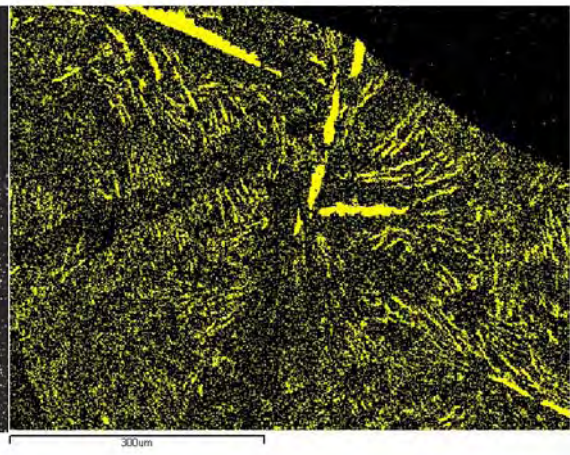
Fig. 4-3b Ag mapping of the same area in Fig. 4-3a. Secondary Ag_3Sn and ternary Ag_3Sn are revealed.
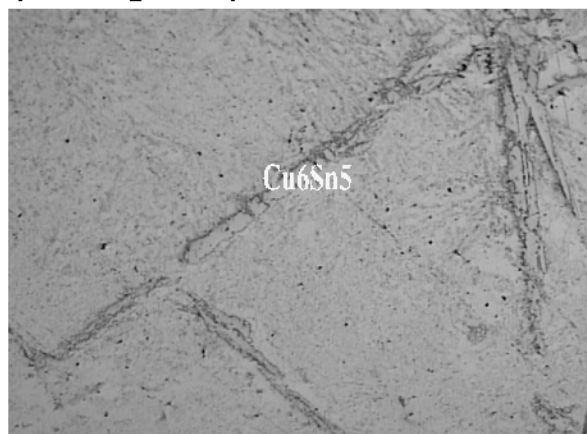
Fig. 4-3c Optical microstructure in the Ames alloy. Large primary Cu_6Sn_5 crystals in Ames alloy.
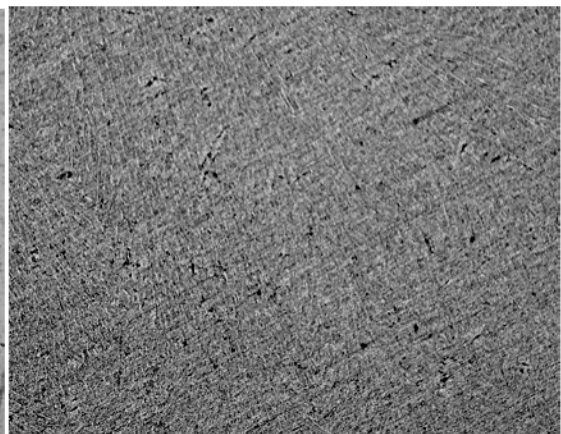
Fig. 4-4. Optical microstructure of HUT eutectic Sn-Ag-Cu alloy (Sn-3.4Ag-0.8Cu).

4.2.2 Comparison of HUT alloy and Ames alloy

In order to see the effects of composition on mechanical properties, Sn-Ag-Cu alloys with the eutectic composition of Sn-3.4Ag-0.8Cu determined by Helsinki University of Technology (HUT) (referred as HUT alloy hereafter) and Ames Lab (Sn-4.7Ag-1.7Cu [140,141], referred as Ames alloy hereafter) were compared in terms of shear strength, creep behavior, and microstructure. Rigid low carbon steel was used to make pins for the grooved lap joints. Solder joints were cooled in glycerol at a cooling rate that was slow enough to let IMC crystals form and grow.

Fig. 4-5 shows the joint appearance of the two alloys. HUT alloy has fine eutectic microstructure but Ames alloy has the plate like IMCs inside the joint. The plate-like IMC crystals make the material and hence the solder joints harder and more brittle. **Fig. 4-6** and **Fig. 4-7** present the shear strength and creep behavior of the two alloys. Each alloy had two samples. HUT alloy had higher shear strength. It should be noted that the shear strength is variable with the change of shear speed and the cooling rate after reflow. Thermal aging also has influence on the shear strength [23]. HUT alloy also had better creep behavior than the Ames alloy. This difference is not surprising because the coarsened primary and secondary IMCs in the Ames alloy degrades the creep property of the joints. The creep behavior is not greatly dependent on cooling rate or external conditions.

4.3 Design of Sn-Ag-Cu solder composition

Although the eutectic SnAgCu solder possesses overall good mechanical properties, it is not necessarily the best for all applications. To design a solder alloy for a specific application one needs to consider several factors such as surface finish materials, substrate and/or PWB thicknesses, package structures, die size and thickness which could change the joint stress situations.
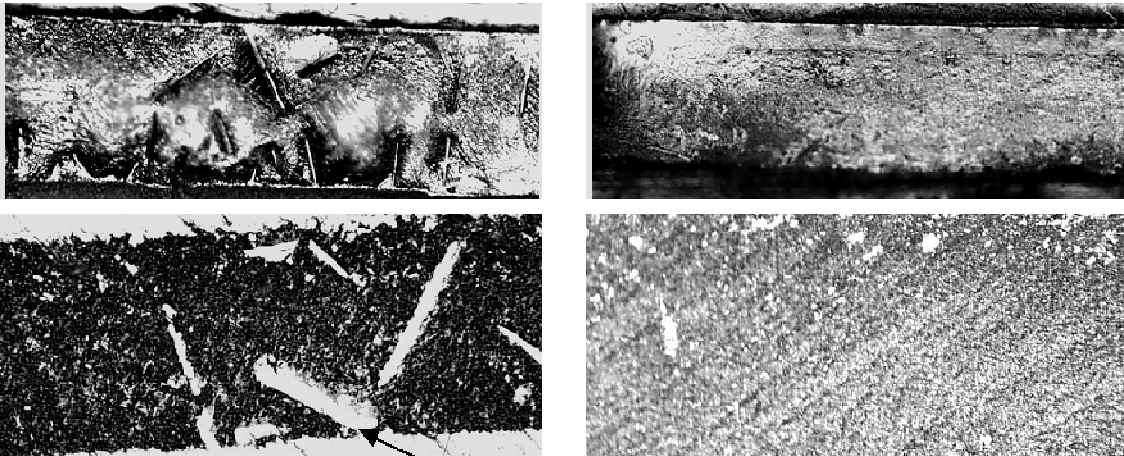
Fig. 4-5 External appearance (upper pictures) and cross section of Sn-Ag-Cu solder joints bottom pictures). Left column: Ames solder. Plate-like IMC are clearly seen. Right column: HUT solder joint. No plate-like IMC was found. Both joints were cooled in Glycerol.

Elastic modulus of the SnAgCu solder increases with Ag content. The elastic modulus of Sn4.0Ag0.5Cu solder is 53.3 GPa, but it is 47 GPa for Sn1.0Ag0.5Cu. In comparison, it is 40.2 GPa for SnPb eutectic solder [54]. This indicates that the lower the Ag content, the softer the SnAgCu solder balls.

During drop tests of BGA package assemblies (**Fig. 2-5b**), a PWB assembly experiences high frequency bending [13] and the solder joints are under tensile stress. Under this condition, if the bulk solder is stiff, the stress is concentrated in the corner area between solder ball and UBM pad, and leads to interfacial fracture. If the solder can deform to such an extent that the stress is at least partially released, the joints will fail at a later time at the interface or within the bulk solder by ductile fracture. However, during thermal cycling, the BGA joints are mainly under shearing stress due to the smaller CTE mismatch between PWB and BGA substrate. The failure mode is usually fatigue of bulk solder. In this situation, high Ag solder has a higher thermal cycling (T/C) performance. This is because more Ag_3Sn particles in solder slow down the propagation of the micro cracks and the solder is more resistant to thermal fatigue. Therefore, for BGA assembly interconnections whose main requirement is thermal

cycling performance, a high Ag content solder is preferred, but it should be lower than 3.5 wt. % to avoid formation of large plates of Ag_3Sn. The low Ag solder is better for drop performance of BGA package assemblies [51].
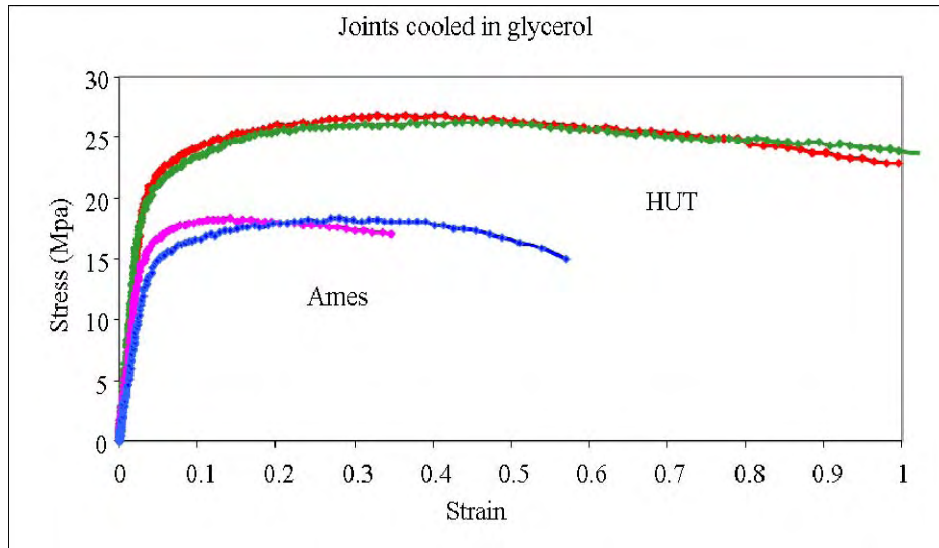
Fig. 4-6 Shear stress at room temperature. Joint cooled in Glycerol.
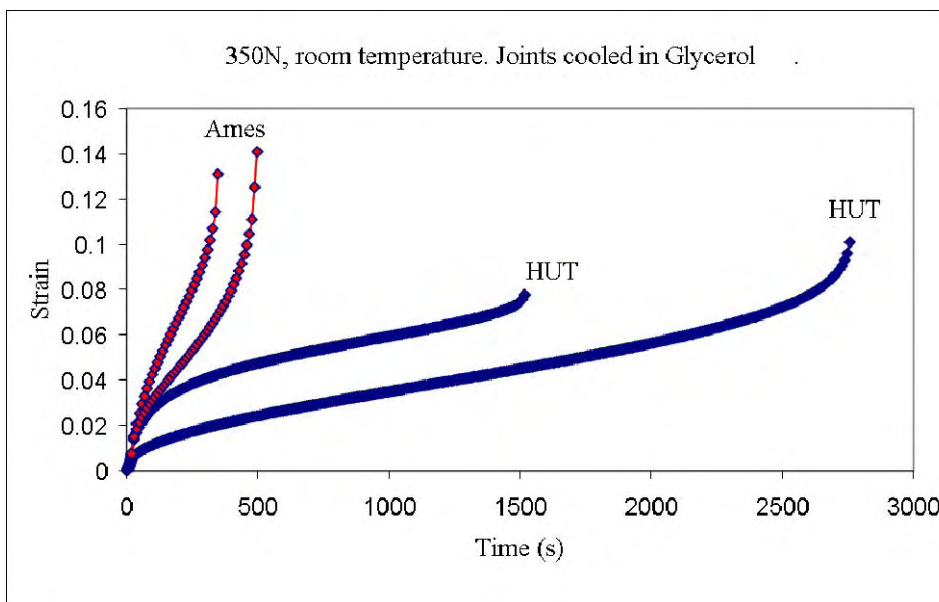
Fig. 4-7 Creep behavior of joints tested under 350N at room temperature. Joints cooled in Glycerol

For WLCSP, the situation is somewhat different. The solder joints are located between two materials that have a larger CTE mismatch (see **Fig. 2-5a**). Since the Si die is rigid, when the temperature increases, the PWB bends much more than in a BGA-PWB assembly and causes higher stress on solder joints. After multiple reflows, the PWB warpage will increase. As a result, the solder balls of WLCSP are under much higher tensile stress than BGA solder balls during reflow and thermal cycling, as schematically illustrated in **Fig. 4-8**. Therefore, the thermal cycling performance of WLCSP was mainly determined by the tensile stress in the solder joints rather than the shear stress as in the BGA packages. Consequently, the effect of Ag content of solder joints on thermal cycling performance of WLCSP was similar to that on drop performance of BGA packages. A low Ag solder gave better thermal cycling performance.
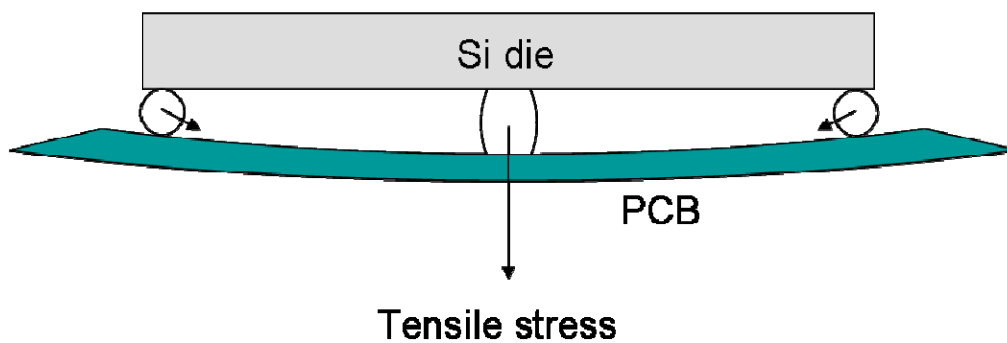
Fig. 4-8 Schematic illustration of stress situation in solder joints at the high temperature dwell of thermal cycling.

PWB thickness in WLCSP also plays an important role. At a given temperature, the stress caused by PWB warpage strongly depends on its thickness. It is more difficult to bend a thick PWB to the same level of warpage than a thinner PWB. As a result, the PWB warpage resulted in high tensile stress in solder joints. In order to improve the package reliability, a soft solder is required to release the tensile stress.

Similar to Ag content, high Cu content in solder increases Cu_6Sn_5 IMC and thus increases the elastic module of the solder balls. If Ni/Au plating is used as discussed in section **3.2.1**, a small variation of Cu content in the range of 0.2-0.6 wt.% can alter

interfacial IMC formation, morphology, thickness and eventually the joint reliability [9-11,145].

5. Evaluation methods for package interconnection reliability

Evaluation methods for package interconnection reliability usually have their standard specifications published by JEDEC (http://www.jedec.org) and IPC (http://www.ipc.org). Companies like Nokia and Motorola have their own test specifications with special objectives. The test plans are typically constructed with many variables so that the reliabilities of different combinations of the variables can be compared. Mechanical loading stress and temperature are most common variables used for reliability tests. The raw data obtained from the tests can be analyzed by statistical methods such as Weibull analysis. In this study, JEDEC standard drop test was carried out and Weibull analysis was employed to analyze the raw data of Pb-free assembly performance. Isothermal aging at different temperatures was applied to solder joints to examine the effect of temperature on joint microstructure and reliability. To study potential risks of Sn-pest in Pb-free solders, low temperature storage was selected. In addition, a thermal cycling test was used to compare Pb-free and Sn-Pb solder joint ability of withstanding thermo-mechanical stresses induced by high and low temperature extremes. Given below are brief descriptions of the drop test, thermal aging, low temperature storage, thermal cycling and Weibull statistic analysis.

5.1 Drop test

Drop test is a technique for measuring the durability of an assembly or device by subjecting it to a free fall from a predetermined height to a surface under prescribed conditions. **Fig. 5-1** shows the schematic view of a drop tester with the sample mounted and the layout of the test board in this work. The test board is screw-mounted to the drop table at 4 corners with the packages facing downwards (**Fig. 5-1b**). Integrity of interconnection in the test board is monitored by in-situ measurement of electrical

resistivity. The test specifications and criteria for failure, based on JEDEC standard JESD22-B111 [146], are listed below:

Peak acceleration: 1500 g +/- 10 %

Pulse duration: 1.0 ms +/- 10 %

Pulse shape: Half-sine waveform

Failure criteria: Electric resistance >1500Ω

Drop height: 1.4 m

Failed daisy chain: Electric resistance >1500Ω for more than 3 drops in a roll of 5
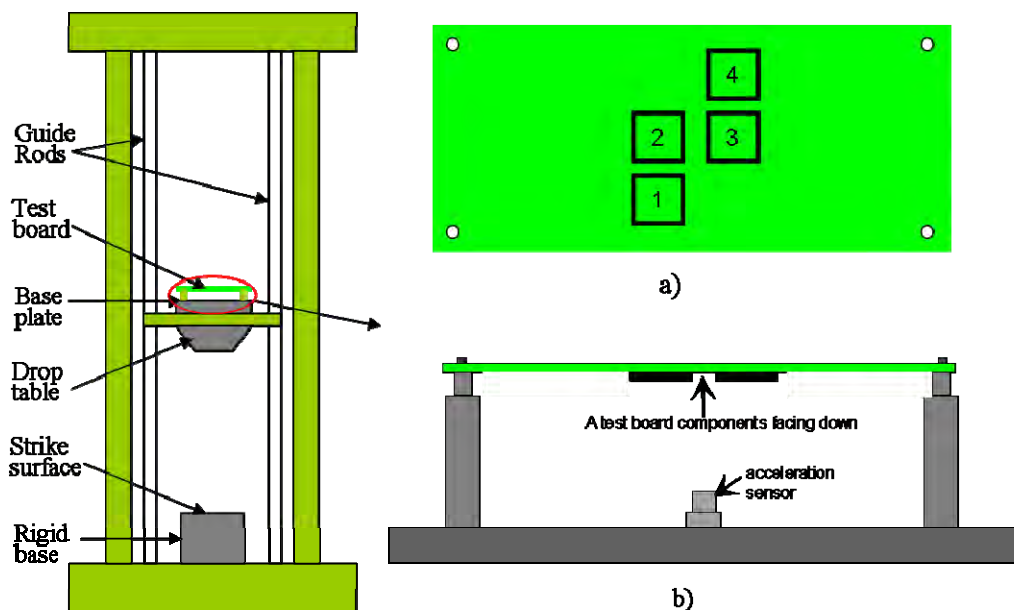
Fig. 5-1 Schematic view of the drop tester with sample mounted and the layout of test board. a) Top view of test board and location of the components. b) Test board mounted on the drop tester.

JESD22-B111 is a board level drop test standard. Many drop test studies are carried out with this specification. Marjamäki and Kivilahti [13] measured the longitudinal strain in the middle of the board layout on the opposite side of the board from the components

(**Fig. 5-2a**). The macroscopic oscillation was due to the natural mode with the lowest frequency. Oscillations at higher frequencies were embedded in the larger strains. The strains due to natural modes with higher frequencies are shown in **Fig. 5-2b**, which presents only the 0 - 5 ms time interval from **Fig. 5-2a**.
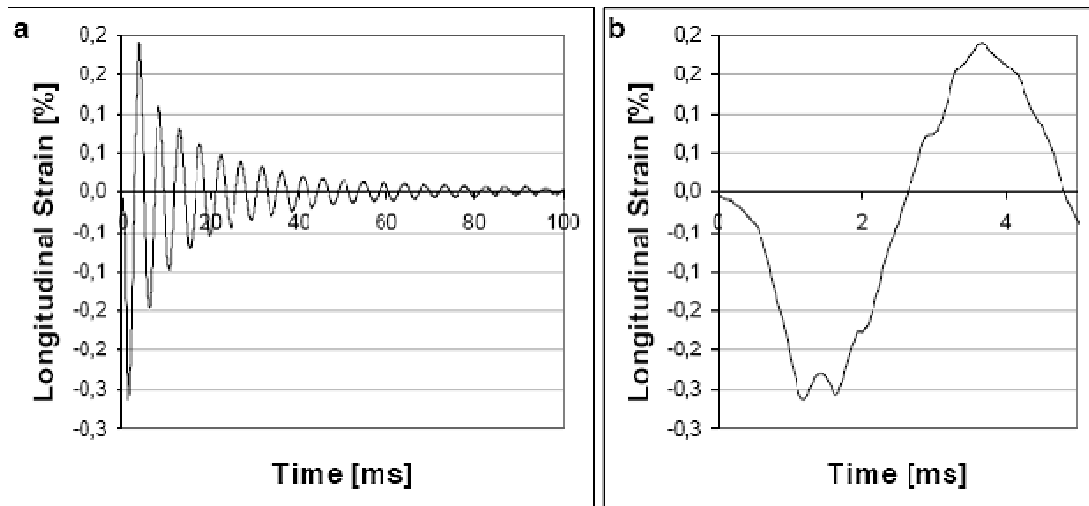
Fig. 5-2 Measured longitudinal strain at the center of the board [13].

All failures after each drop were logged. A total of 5 packages from the test lot were subjected to failure analysis to determine the root cause and to identify failure mechanism. The selection of packages covers different locations on the board. Different methods and equipment, such as visual inspection, cross-section, dye and pry, chemical etching, SEM, and FIB were employed to determine the root cause of failure. The failure site was clearly identified as "component failure", "interconnect failure", or "board failure" to identify the weakest interface or point.

In order to identify the initial failure modes by drop test, one board was pulled out after the first failure occurred in any of the components during the drop test. The rest of the boards continued to be further tested until all the components failed or reach a pre-determined drop numbers, such as 400 drops. Thus, a lot of data is obtained for Weibull analysis.

5.2 Thermal aging

Some of functional components reached a temperature up to 120ºC during long term service; the purpose of the thermal aging test is to accelerate this process to expose the package assemblies to an isothermal condition for a preset period of time. In this work [8,105], Chip scale packages (CSPs) were assembled on PWB and thermally aged at 100, 125, and 150 °C for up to 1000 h. The temperatures were controlled to an accuracy of ±2ºC. To avoid influence of materials from the other side of the joints, both PWB and CSP pads were OSP coated Cu. The solder balls were of Sn–3.8Ag–0.7Cu.

5.3 Low temperature storage

In the past, tin pest has not been a problem in solder joint because the solder used for device assembly was a Sn-Pb alloy that contained about 40 wt.% Pb. Pb is an effective element at inhibiting the transformation of β-Sn to α-Sn. In Pb-free solders, Sn content is up to 95-99 wt.%. This raises a concern of whether or not the tin pest could occur in the Pb-free solder joints in electronic packages, especially for those that work outdoors, where the environmental temperature could be lower than 13°C. For example, in the north of the Nordic countries, the highest outdoor temperature in winter is only 8°C. If the Sn pest happens to the solder joints in electronic packages, obviously it would cause failure of the device.

To find out whether the Sn pest happens in Pb-free solder joints or not, low temperature storage was carried out to speed up the Sn allotropic transformation. The alloy ingots were cold rolled to be ~1 mm thick. The reduction was about 80%. Samples were cut from the rolled plates for the low temperature storage test. They were first stored in liquid nitrogen of at −196ºC for 50 hours. After surface examination, they were stored at −40ºC for four years. Surface examination of the samples was performed after each year. Then, they were stored at −17ºC for 1.5 years.

5.4 Thermal cycling

Thermal cycling was conducted to determine the ability of the assemblies and solder interconnects to withstand mechanical stresses induced by alternating high and low temperature extremes. Permanent changes in electrical and/or physical characteristics can result from these mechanical stresses. Usually dual chamber cycling was used for the solder interconnection cycles; the assemblies are placed on a moving platform that shuttles between stationary chambers maintained at fixed temperatures. Typical solder interconnect cycle rates are slower, in the range of 1 to 2 cycles per hour (cph), when solder joint fatigue evaluations are performed. These include CSP, WLCSP, BGA and stacked packages with solder interconnections. Cycle frequency and soak time is more significant for solder interconnections. Cycle time between one high temperature extreme to the next, or from one low temperature extreme to the next, for given samples shown in **Fig. 5-3** from JESD22-A104C [147].
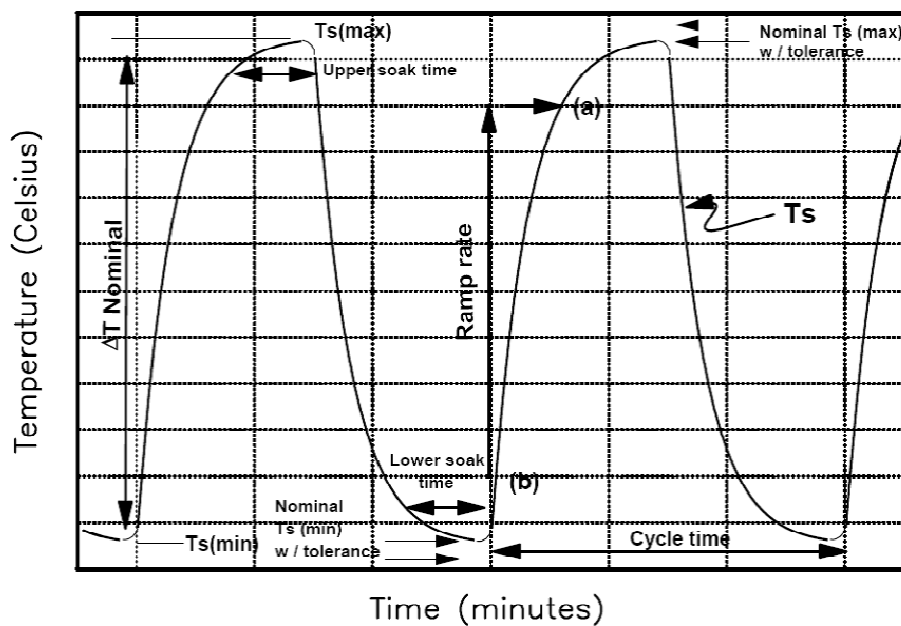
Fig. 5-3 Representative temperature profile for thermal cycle test conditions. Ts(max) is the temparture of the sample required to meet the maximum nominal temperature for a specific test condition. Ts(min) is the temperature of the sample required to meet norminal temperature for a specific test condition. (courtesy by JESD22-A104C)

Samples in Publication IV of this dissertation were leadless organic and ceramic chip carrier components. The assemblies were thermal cycled between –40 and 85ºC, with 14 minute dwells at the temperature extremities, and three minute ramps. The thermal cycling temperature range used in the simulation in Publication VI of this dissertation was –40°C to 125°C.

5.5 Weibull analysis

Weibull distribution was first published by a Swedish statistician Waloddi Weibull in 1939 and developed by him in 1951 [148]. Weibull distribution is widely used in reliability and life data analysis due to its versatility. Depending on the values of the parameters, the Weibull distribution can be used to model a variety of life behaviors. The Weibull probability density function and cumulative density function as well as their associated parameters are discussed below.

5.5.1 Reliability bathtub curve

Package interconnection reliability is the ability of the package to operate without failure under a set of predetermined conditions over a specified period of time. Most packages exhibit failure characteristics as shown in the bathtub curve of **Fig. 5-4**. This curve is plotted with the package life on the x-axis and the failure rate on the y-axis. The life can be in minutes, hours, years, cycles, number of drops, actuations or any other quantifiable unit of time or use. The failure rate is given as failures among surviving units per time unit. As can be seen from this plot, many packages will begin their lives with a higher failure rate (which can be due to manufacturing defects, poor workmanship, poor quality control of incoming parts, etc.) and exhibit a decreasing failure rate. The failure rate then usually stabilizes to an approximately constant rate in the useful life region, where the failures observed are chance or random failures. As the packages experience more use and wear, the failure rate begins to rise as the population begins to experience failures related to wear-out. This is similar to the case of human mortality, the mortality rate (failure rate), is higher during the first year or so of life,

then drops to a low constant level during our teens and early adult life and then rises as we progress in years.
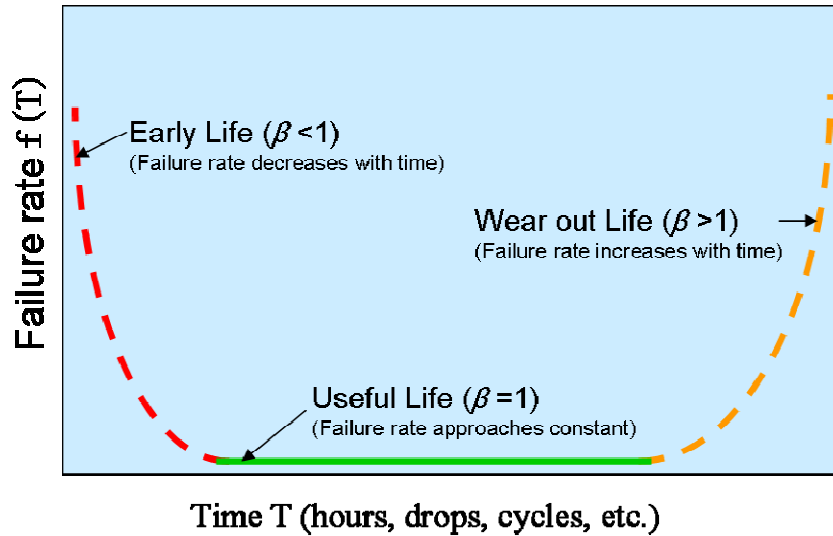
Fig. 5-4 An idealized reliability bathtub curve, with the three major life regions: early, useful and wear out. β is Weibull shape parameter.

5.5.2 Weibull distribution

The three life–stages of the reliability bathtub curve can thus be mathematically represented with the Weibull distribution by means of the parameter β. When the β value is less than unity the plot represents "infant mortality" failures, when β equals one the plot represents the failures during the "useful lifetime", and when β is greater than one the distribution represents the "wear–out" failures. The Weibull probability density function and the cumulative distribution function are given by

$$f(T) = \frac{\beta}{\eta}\left(\frac{T-\gamma}{\eta}\right)^{\beta-1} e^{-\left(\frac{T-\gamma}{\eta}\right)^{\beta}} \quad (7)$$

where $f(T) \geq 0$, $T \geq 0$ or γ, $\beta > 0$, $\eta > 0$, $-\infty < g < \infty$

η = scale parameter,

β = shape parameter (or slope),

γ = location parameter.

In general, most distributions used for reliability and life data analysis, the lifetime distributions, are usually limited to a maximum of the above three parameters. **Fig. 3-2** is an example of the Weibull plotting of drop test data at time 0 and after thermal aging at 100, 125, and 150ºC for 200 hours. Shape and scale parameters for each test condition are listed in the embedded table. Location parameter is at 10 drops.

Scale Parameter. The scale parameter η is the most common type of parameter. It is also called the characteristic life; it can be read from the diagram at the 63.2% cumulative failure rate of the regression line. The scale parameter defines where the bulk of the distribution lies, or how stretched out the distribution is. **Fig. 3-3** shows the characteristic life is 76.69-106.4 drops for the four tested groups.

Shape parameter. The shape parameter β, as the name implies, helps define the shape of a distribution. It is also known as the slope. This is because the value of β is equal to the slope of the regression line in a probability plot. The effect of the shape parameter on a distribution is reflected in the shapes of the probability density function, the reliability function and the failure rate function. The value of $\beta = 1$ divides the behavior of the Weibull function: values of $\beta < 1$ correspond to decreasing failure rate, $\beta = 1$ to constant failure rate, and $\beta > 1$ to increasing failure rate. **Fig. 3-3** shows this graphically and $\beta > 1$ for all four tested groups. Compare β value of 3.020 and 8.209 in **Fig. 3-2**. The larger the β value shows that the plot is more vertical, indicating the failure occurred in a short time period most likely with same failure mode.

The failure mode or mechanism associated with the β parameter has to be determined by physical failure analysis. Ideally, each value of beta depicts a single failure mode, but there may also be several failure modes acting simultaneously, and many different mechanisms may be confounded in the beta (β) value. Thus, each failure mode needs to be identified and a separate analysis should be carried out for each case.

Location parameter *γ* is used to shift a distribution in one direction or another. It defines the location of the origin of a distribution and can be either positive or negative. In terms of lifetime distributions, the location parameter represents a time shift and it is very often zero. If *γ* is equal to 0, the distribution starts at 0 at X-axial or at the origin. In **Fig. 3-3**, the location parameter *γ* is 10 drops. The life period 0 to +γ is a failure free operating period of such units.

In summary, the raw data by reliability tests can be directly inputted into Weibull software program and the Weibull plots can be generated immediately and the three parameters are automatically produced. It can be seen that the group with150ºC/200h thermal aging has better drop performance than other three groups. The rationale was discussed in publication I [8].

6. Summary

This dissertation, "An Investigation of Reliability of High Density Electronic Package-to-Board Interconnections from the Perspective of Solder Joint Metallurgy" consists of six publications and part of the licentiate degree thesis [23]. The objective of the dissertation was to understand the relationship between microstructure and solder joint reliability under different loading conditions. The statistical Weibull distribution method was used for drop and thermal cycling data analysis. The BLR of assemblies strongly depends on microstructure of the solder joints. This can be expressed as a complex relationship: among materials and/or alloy composition and/or process → microstructure change in bulk solder and/or interface → solder joint reliability variation. By changing the loading conditions such as temperature, time, environment, or materials like solder composition and surface materials, the microstructure of the solder joints changes, resulting in different reliability performance.

The main findings of this investigation are:

1) The interfacial IMCs in SnAgCu solder joints with bare Cu or OSP-Cu are Cu_6Sn_5 and Cu_3Sn, the same as in the SnPb solder joints. The type of interfacial IMCs in SnAgCu solder joints on Ni/Au plating depends on the Cu content of the solder. If the Cu content is less than 0.3 wt.%, $(Ni,Cu)_3Sn_4$ forms. When the Cu content is higher than that, both $(Cu,Ni)_6Sn_5$ and $(Ni,Cu)_3Sn_4$ may form. The dual IMC structure of $(Cu,Ni)_6Sn_5/(Ni,Cu)_3Sn_4$ might be the root cause for the high interfacial failure rate of SnAgCu solder joints.

2) Thermal aging changed Pb-free solder joint microstructures and directly contributed to the joint drop performance. Proper thermal aging can be applied to improve joint reliability up to 50%. Dispersion strengthening of IMCs, microstructure coarsening of the IMC particles, strain rate hardening, solder fatigue, and recrystallization of Sn grains at the stressed areas were observed and those were true factors that directly impact drop performance of the Pb-free solder joints.

3) Micro-voiding at Cu/Cu_3Sn interface doesn't cause drop failures in this study. The weakest interfaces were Cu_3Sn/Cu_6Sn_5 and $Cu_6Sn_5/Solder$. With increased aging, temperature and time, the weakest interface shifted from the intermetallic layer to the bulk solder. The thickness of Cu_3Sn significantly increased with aging, but that of Cu_6Sn_5 changed only a little. The interfacial Cu_3Sn layer was found to grow at the expense of Cu_6Sn_5.

4) Eutectic alloy was designed by thermodynamic calculations and experimentally determined to be Sn-3.4Ag-0.8Cu, In comparison to non-eutectic alloys, Sn-3.4Ag-0.8Cu alloy showed overall better performance in regard to shear stress and creep behaviors. Cooling rate after reflow plays an important role.

5) Sn-2.5Ag-0.8Cu-0.5Sb and Sn-Pb-2Ag solder joints exhibited different failure mechanisms in the presence of gold in thermal cycling. Cracks in the lead-free joints propagated along the boundaries of Au-Sn and Ag-Sn intermetallics, while they propagated through the Pb-rich layer at the solder-component interface in the Sn-Pb-

2Ag solder joints. The effect of high Au content (15 wt.%) on lead free solder joint reliability is not resolved.

6) Tin pest is less likely to cause failure of Pb-free solder joints in mobile electronic devices, but pure tin is not recommended for the products that are to be used outdoor in the cold regions such as Nordic countries where the temperature in winter can be as low as −40ºC.

In this work, the study for the package-to-board interconnections was focused on the solder ball size larger than 250 μm. For future solder joint interconnections or different levels of package interconnections, further research is needed and the relationship chain can be used to explain complex reliability performances of the high density electronic package interconnections.

7. References

[1]   C. Liu, M. W. Hendriksen, D. A. Hutt, P. P. Conway, and D. C. Whalley, "Materials and processes issues in fine pitch eutectic solder flip chip interconnection," *IEEE Trans. Compon. Packag. Technol.* , **29**, 4, (2006), pp. 869-877.

[2]   E. D. Perfecto, D. Hawken, H. P. Longworth, H. Cox, K. Srivastava, V. Oberson, J. Shah, and J. Garant, "C4NP technology: Manufacturability, yields and reliability," *The Proceedings of the 58th Electr. Compon. Technol. Conf.*, Lake Beuna Vista, FL, USA, May 27-30, 2008, IEEE, (2008), pp. 1641-1647.

[3]   E. Laine, K. Ruhmer, E. Perfecto, H. Longworth, and D. Hawken, "C4NP as a high-volume manufacturing method for fine-pitch and lead-free flip hip solder bumping " *The Proceedings of the 1st Electr. SystemIntegration Technol. Conf.*, Dresden, Germany, Sept. 5-7, 2006, IEEE, (2006), pp. 518-524.

[4]   W. Zhou, Y. P. Chia, and S. W. Low, "Development of fine pitch solders joint interconnection technology for flip chip assembly," *The Proceedings of the 7th Electr. Packag. Technol. Conf.*, Singapore, Dec. 7-9, 2005, IEEE, (2005), pp. 509-515.

[5]   B. Dang, D.-Y. Shih, S. Buchwalter, C. Tsang, C. Patel, J. Knickerbocker, P. Gruber, S. Knickerbocker, J. Garant, K. Semkow, K. Ruhmer, and E. Hughlett, "50μm pitch Pb-free micro-bumps by C4NP technology," *The Proceedings of the 58th Electr. Compon. Technol. Conf.*, Lake Beuna Vista, FL, USA, May 27-30, 2008, IEEE, (2008), pp. 1505-1510.

[6]   S. Wakiyama, H. Ozaki, Y. Nabe, T. Kume, T. Ezaki, and T. Ogawa, "Novel low-temperature CoC interconnection technology for multichip LSI (MCL)," *The Proceedings of the 57th Electr. Compon. Technol. Conf.*, Reno, Nevada, USA, May 29 - June 1, 2007, IEEE, (2007), pp. 610-615.

[7]   S. K. Kang, R. S. Rai, and S. Purushothaman, "Interfacial reactions during soldering with lead-tin eutectic and lead (Pb)-free, tin-rich solders," *J. Electr. Mater.*, **25**, 7, (1996), pp. 1113-1120.

[8]   W. Peng and M. E. Marques, "Effect of thermal aging on drop performance of chip scale packages with SnAgCu solder joints on Cu pads," *J. Electr. Mater.*, **36**, 12, (2007), pp. 1679-1690.

[9]   C. E. Ho, R. Y. Tsai, Y. L. Lin, and C. R. Kao, "Effect of Cu concentration on the reactions between Sn-Ag-Cu solders and Ni," *J. Electr. Mater.*, **31**, 6, (2002), pp. 584-590.

[10]   J. Y. Kim, Y. C. Sohn, and Y. Jin, "Effect of Cu content on the mechanical reliability of Ni/Sn-3.5Ag system," *J. Mater. Res.*, **22**, 3, (2007), pp. 770-776.

[11]   C. H. Wang and S. W. Chen, "Sn-0.7 wt.%Cu/Ni interfacial reactions at 250°C," *Acta Mater.*, **54**, 1, (2006), pp. 247-253.

[12]   K. Zeng and K. N. Tu, "Six cases of reliability study of Pb-free solder joints in electronic packaging technology," *Mater. Sci. Eng. R: Reports*, **38**, 2, (2002), pp. 55-105.

[13]   P. Marjamaki, T. T. Mattila, and J. K. Kivilahti, "A comparative study of the failure mechanisms encountered in drop and large amplitude vibration tests," *The Proceedings of the 56th Electr. Compon. Technol. Conf.*, San Diego, CA, USA, May 30 - June 2, 2006, IEEE, (2006), pp. 95-101.

[14]   T. T. Mattila, P. Marjamaki, L. Nguyen, and J. K. Kivilahti, "Reliability of chip scale packages under mechanical shock loading," *The Proceedings of the 56th Electr. Compon. Technol. Conf.*, San Diego, CA, USA, May 30 - June 2, 2006, IEEE, (2006), pp. 584-589.

[15]   T. Y. Lee, K. N. Tu, S. M. Kuo, and D. R. Frear, "Electromigration of eutectic SnPb solder interconnects for flip chip technology," *J. Appl. Phys.*, **89**, 6, (2001), pp. 3189-3194.

[16]   H. Ye, C. Basaran, and D. Hopkins, "Thermomigration in Pb–Sn solder joints under joule heating during electric current stressing," *Appl. Phys. Lett.*, **82**, 7, (2003), pp. 1045-1047.

[17]   Y. C. Hu, Y. H. Lin, C. R. Kao, and K. N. Tu, "Electromigration failure in flip chip solder joints due to rapid dissolution of copper," *J. Mater. Res.*, **18**, 11, (2003), pp. 2544-2548.

[18]   D. Q. Yu, W. Jillek, and E. Schmitt, "Electrochemical migration of lead free solder joints," *J. Mater. Sci.: Mater. Electr.*, **17**, 2, (2006), pp. 229-241.

[19]   S. Canumalla, K. Ludwig, R. Pedigo, and T. Fitzgerald, "A study on ranking of commercial fluxes for electrochemical migration (ECM) propensity for Cu, Sn and Ag surface finishes," *The Proceedings of the 56th Electr. Compon. Technol. Conf.*, San Diego, CA, USA, May 30 - June 2, 2006, IEEE, (2006), pp. 625-632.

[20]   L. K. Teh, M. Teo, E. Anto, C. C. Wong, S. G. Mhaisalkar, P. S. Teo, and E. H. Wong, "Moisture-induced failures of adhesive flip chip interconnects," *IEEE Trans. Compon. Packag. Technol.*, **28**, 3, (2005), pp. 506-516.

[21]   W. J. Plumbridge, "Tin pest issues in lead-free electronic solders," *J. Mater. Sci.: Mater. Electr.*, **18**, 9, (2007), pp. 307-318.

[22]   W. J. Plumbridge, "Recent observations on tin pest formation in solder alloys," *J. Electr. Mater.*, **37**, 2, (2008), pp. 218-223.

[23]   W. Peng, "Lead-free electronic assembly based on Sn-Ag-Cu solders," Licentiate Thesis, Helsinki University of Technology, Helsinki, Finland (2001).

[24]   M. E. Loomans and M. E. Fine, "Tin-silver-copper eutectic temperature and composition," *Metall. Mater. Trans. A*, **31A**, 4, (2000), pp. 1155-1162.

[25]   K.-W. Moon, W. J. Boettinger, U. R. Kattner, F. S. Biancaniello, and C. A. Handwerker, "Experimental and thermodynamic assessment of Sn-Ag-Cu solder alloys," *J. Electr. Mater.*, **29**, 10, (2000), pp. 1122-1136.

[26]   D. Lewis, S. Allen, M. Notis, and A. Scotch, "Determination of the eutectic structure in the Ag-Cu-Sn system," *J. Electr. Mater.*, **31**, 2, (2002), pp. 161-167.

[27]   V. Vuorinen, "Interfacial reactions between Sn-based solders and common metallisations used in electronics," PhD Thesis, Helsinki University of Technology, Helsinki, Finland (2006).

[28]   P. Oberndorff, "Lead-free solder systems: Phase relations and microstructure," PhD Thesis, Eindhoven University of Technology, Eindhoven, The Netherland (2001).

[29]   A. Syed, T.-S. Kim, S.-W. Cha, J. Scanion, and C.-G. Ryu, "Effect of Pb free alloy composition on drop/impact reliability of 0.4, 0.5 and 0.8mm pitch chip scale packages with NiAu pad finish," *The Proceedings of the 57th Electr. Compon. Technol. Conf.*, Reno, NV, USA, May 29 - June 1, 2007, IEEE, (2007), pp. 951-956.

[30]   Y. S. Lai, P. F. Yang, and C. L. Yeh, "Experimental studies of board-level reliability of chip-scale packages subjected to JEDEC drop test condition," *Microelectr. Reliab.*, **46**, 2-4, (2006), pp. 645-650.

[31]   P.-W. Kim, B.-S. Kim, E.-C. Ahn, and T.-G. Chung, "Improvement of drop reliability in OSP/Cu pad finished packages," *The Proceedings of the 8th Electr. Packag. Technol. Conf.*, Singapore, Dec. 6-8, 2006, IEEE, (2006), pp. 168-173.

[32]   Y.-S. Lai, P.-F. Yang, C.-L. Yeh, and C.-I. Tsai, "Board-level drop performance of lead-free chip-scale packages with different soldermask openings and solder compositions," *The Proceedings of the 6th Int. Conf. Electr. Mater. Pack.*, Penang, Malaysia, Dec. 5-7, 2004, IEEE, (2004), pp. 56-60.

[33]   H. Kim, M. Zhang, C. M. Kumar, D. Suh, P. Liu, D. Kim, M. Xie, and Z. Wang, "Improved drop reliability performance with lead-free solders of low Ag content and their failure modes," *The Proceedings of the 57th Electr. Compon. Technol. Conf.*, Reno, Nevada, USA, May 29 - June 1, 2007, IEEE, (2007), pp. 962-967.

[34]   D. W. Henderson, J. J. Woods, T. A. Gosselin, J. Bartelo, D. E. King, T. M. Korhonen, M. A. Korhonen, L. P. Lehman, E. J. Cotts, S. K. Kang, P. Lauro, D. Y. Shih, C. Goldsmith, and K. J. Puttlitz, "The microstructure of Sn in near-eutectic Sn-Ag-Cu alloy solder joints and its role in thermomechanical fatigue," *J. Mater. Res.*, **19**, 6, (2004), pp. 1608-1612.

[35]   M. A. Matin, E. W. C. Coenen, W. P. Vellinga, and M. G. D. Geers, "Correlation between thermal fatigue and thermal anisotropy in a Pb-free solder alloy," *Scr. Mater.*, **53**, 8, (2005), pp. 927-932.

[36] K. N. Subramanian and J. G. Lee, "Effects of internal stresses on the thermomechanical behavior of Sn-based solder joints," *Mater. Sci. Eng. A*, **A421**, 1-2, (2006), pp. 46-56.

[37] S. Terashima, M. Tanaka, and K. Tatsumi, "Thermal fatigue properties and grain boundary character distribution in Sn-xAg-0.5Cu (x=1, 1.2 and 3) lead free solder interconnects," *Sci. Technol. Welding and Joining*, **13**, 1, (2008), pp. 60-65.

[38] S. Choi, K. N. Subramanian, J. P. Lucas, and T. R. Bieler, "Thermomechanical fatigue behavior of Sn-Ag solder joints," *J. Electr. Mater.*, **29**, 10, (2000), pp. 1249-1257.

[39] C. Kanchanomai, Y. Miyashita, and Y. Mutoh, "Low-cycle fatigue behavior of Sn-Ag, Sn-Ag-Cu, and Sn-Ag-Cu-Bi lead-free solders," *J. Electr. Mater.*, **31**, 5, (2002), pp. 456-465.

[40] X. W. Liu and W. J. Plumbridge, "Damage produced in solder alloys during thermal cycling," *J. Electr. Mater.*, **36**, 9, (2007), pp. 1111-1120.

[41] M. A. Matin, W. P. Vellinga, and M. G. D. Geers, "Thermomechanical fatigue damage evolution in SnAgCu solder joints," *Mater. Sci. Eng. A*, **445-446**, 1, (2007), pp. 73-85.

[42] J. K. Shang, Q. L. Zeng, L. Zhang, and Q. S. Zhu, "Mechanical fatigue of Sn-rich Pb-free solder alloys," *J. Mater. Sci.: Mater. Electr.*, **18**, 1, (2007), pp. 211-227.

[43] Q. L. Zeng, Z. G. Wang, A. P. Xian, and J. K. Shang, "Cyclic softening of the Sn-3.8Ag-0.7Cu lead-free solder alloy with equiaxed grain structure," *J. Electr. Mater.*, **34**, 1, (2005), pp. 62-67.

[44] M. Kerr and N. Chawla, "Creep deformation behavior of Sn–3.5Ag solder/Cu couple at small length scales," *Acta Mater.*, **52**, 15, (2004), pp. 4527–4535.

[45] T. Chen and I. Dutta, "Effect of Ag and Cu concentrations on the creep behavior of Sn-based solders," *J. Electr. Mater.*, **37**, 3, (2008), pp. 347-354.

[46] R. S. Sidhu and N. Chawla, "Thermal fatigue behavior of Sn-Rich (Pb-Free) solders," *Metall. Mater. Trans. A*, **39A**, 4, (2008), pp. 799-810.

[47] K. Suganuma, S. H. Huh, K. Kim, H. Nakase, and Y. Nakamura, "Effect of Ag content on properties of Sn-Ag binary alloy solder," *Mater. Trans.*, **42**, 2, (2001), pp. 286-291.

[48] D. W. Henderson, T. Gosselin, A. Sarkhel, S. K. Kang, W.-K. Choi, D.-Y. Shih, C. Goldsmith, and K. J. Puttlitz, "Ag3Sn plate formation in the solidification of near ternary eutectic Sn-Ag-Cu alloys," *J. Mater. Res.*, **17**, 11, (2002), pp. 2775-2778.

[49] K. S. Kim, S. H. Huh, and K. Suganuma, "Effects of intermetallic compounds on properties of Sn-Ag-Cu lead-free soldered joints," *J. Alloys Compd.*, **352**, 1-2, (2003), pp. 226-236.

[50] C. Zhang, J.-K. Lin, and L. Li, "Thermal fatigue properties of lead-free solders on Cu and Ni(P) under bump metallurgies," *The Proceedings of the 51st Electr. Compon. Technol. Conf.*, Orlando, Florida, May 29-June 31, 2001, IEEE, (2001), pp. 457-464.

[51] M. Amagai, Y. Toyoda, and T. Tajima, "High solder joint reliability with lead-free solders," *The Proceedings of the 53rd Electr. Compon. Technol. Conf.*, New Orleans, USA, May 27-30, 2003, IEEE, (2003), pp. 317-322.

[52] J. G. Lee and K. N. Subramanian, "Effects of TMF heating rates on damage accumulation and resultant mechanical behavior of Sn–Ag based solder joints," *Microelectr. Reliab.*, **47**, 1, (2007), pp. 118-131.

[53] E. Orowan, The Proceedings of Symp. Internal Stresses in Metals and Alloys, Session III Discussion, 1948, Institute of Metals, London, England, (1948).

[54] L. Garner, S. Sane, D. Suh, T. Byrne, A. Dani, T. Martin, M. Mello, M. Patel, and R. Williams, "Finding solutions to the challenges in package interconnect reliability," *Intel Technol. J.*, **9**, 4, (2005), pp. 297-308.

[55] A. Lal and E. Bradley, "Relationship of tensile interfacial strength to lead-free BGA impact performance," *The Proceedings of the 56th Electr. Compon. Technol. Conf.*, San Diego, CA, USA, May 30-June 2, 2006, IEEE, (2006), pp. 1628-1633.

[56] A. Syed, T. S. Kim, Y. M. Cho, C. W. Kim, and M. Yoo, "Alloying effect of Ni, Co, and Sb in SAC solder for improved drop performance of chip scale packages with Cu OSP pad finish," *The Proceedings of the 8th Electr. Packag. Technol. Conf.*, Singapore, Dec. 6-8, 2006, IEEE, (2006), pp. 404-411.

[57] L. Xiao, J. Liu, Z. Lai, L. Ye, and A. Tholen, "Characterization of mechanical properties of bulk lead free solders," *The Proceedings of Inter. Symp. Adv. Packag. Mater.: Processes, Properties and Interfaces*, Braselton, GA, USA, March 6-8, 2000, IEEE, (2000), pp. 145-151.

[58] O. Fouassier, J.-M. Heintz, J. Chazelas, P.-M. Geffroy, and J.-F. Silvain, "Microstructural evolution and mechanical properties of SnAgCu alloys," *J. Appl. Phys.*, **100**, 4, (2006), pp. 043519.

[59] X. Long, I. Dutta, V. Sarihan, and D. R. Frear, "Deformation behavior of Sn-3.8Ag-0.7Cu solder at intermediate strain rates: Effect of microstructure and test conditions," *J. Electr. Mater.*, **37**, 2, (2008), pp. 189-200.

[60] P. T. Vianco, J. A. Rejent, and A. C. Kilgo, "Creep behavior of the ternary 95.5Sn-3.9Ag-0.6Cu solder: Part II-aged condition," *J. Electr. Mater.*, **33**, 12, (2004), pp. 1473-1484.

[61] A. Bobe, D. Regener, G. Dietze, and H. Heyse, "Changes of lead free solder joints under thermal loading," *Praktische Metallographie*, **44**, 10, (2007), pp. 476-492.

[62] Q. Xiao, L. Nguyen, and W. D. Armstrong, "Aging and creep behavior of Sn3.9Ag0.6Cu solder alloy," *The Proceedings of the 54th Electr. Compon. Technol. Conf.*, Las Vegas, NV, USA, June 1-4, 2004, IEEE, (2004), pp. 1325-1332.

[63] R. J. McCabe and M. E. Fine, "Athermal and thermally activated plastic flow in low melting temperature solders at small stresses," *Scr. Mater.*, **39**, 2, (1998), pp. 189-195.

[64] W. J. Plumbridge and C. R. Gagg, "Effect of strain rate and temperature on the stress-strain response of solder alloys," *J. Mater. Sci.: Mater. Electr.*, **10**, 5, (1999), pp. 461-468.

[65]   X. Q. Shi, W. Zhou, H. L. J. Pang, and Z. P. Wang, "Effect of temperature and strain rate on mechanical properties of 63Sn/37Pb solder alloy," *J. Electr. Packag.*, **121**, 3, (1999), pp. 179-185.

[66]   J. Liang, N. Dariavach, G. Barr, and Z. Fang, "Effects of strain rates and biaxial stress conditions on plastic yielding and flow stress of solder alloys," *J. Electr. Mater.*, **35**, 2, (2006), pp. 372-379.

[67]   J. Liang, N. Dariavach, and D. Shangguan, "Deformation behavior of solder alloys under variable strain rate shearing & creep conditions," *The Proceedings of Int. Symp. Adv. Packag. Mater.: Processes, Properties and Interfaces*, Irvine, CA, USA, March 16-18, 2005, IEEE, (2005), pp. 21-26.

[68]   T. T. Mattila and J. K. Kivilahti, "Failure mechanisms of lead-free chip scale package interconnections under fast mechanical loading," *J. Electr. Mater.*, **34**, 7, (2005), pp. 969-976.

[69]   K. Newman, "BGA brittle fracture – Alternative solder joint integrity test methods," *The Proceedings of the 55th Electr. Compon. Technol. Conf.*, Lake Buena Vista, FL, USA, May 31-June 3, 2005, IEEE, (2005), pp. 1194-1201.

[70]   F. Song, S. W. R. Lee, K. Newman, S. Clark, and B. Sykes, "Comparison of joint strength and fracture energy of lead-free solder balls in high speed ball shear/pull tests and their correlation with board level drop test," *The Proceedings of the 9th Electr. Packag. Technol. Conf.*, Singapore, Dec. 10-12, 2007, IEEE, (2007), pp. 450-458.

[71]   F. Song, S. W. R. Lee, K. Newman, H. Reynolds, S. Clark, and B. Sykes, "Effect of thermal aging on high speed ball shear and pull tests of SnAgCu lead-free solder balls," *The Proceedings of the 9th Electr. Packag. Technol. Conf.*, Singapore, Dec. 10-12, 2007, IEEE, (2007), pp. 463-470.

[72]   X. Fan, G. Raiser, and V. S. Vasudevan, "Effects of dwell time and ramp rate on lead-free solder joints in FCBGA packages," *The Proceedings of the 55th Electr. Compon. Technol. Conf.*, Lake Buena Vista, FL, USA, May 31-June 3, 2005, IEEE, (2005), pp. 901-906.

[73]   D. Kim, D. Suh, T. Millard, H. Kim, C. Kumar, M. Zhu, and Y. Xu, "Evaluation of high compliant low Ag solder alloys on OSP as a drop solution for the 2nd level Pb-free interconnection," *The Proceedings of the 57th Electr. Compon. Technol. Conf.*, Reno, NV, USA, May 29 - June 1, 2007, IEEE, (2007), pp. 1614-1619.

[74]   F. Zhu, H. Zhang, R. Guan, and S. Liu, "The effect of temperature and strain rate on the tensile properties of a Sn99.3Cu0.7(Ni) lead –free solder alloy," *Microelectr. Eng.*, **84**, 1, (2007), pp. 144-150.

[75]   D. Chan, D. Bhate, G. Subbarayan, D. Love, and R. Sullivan, "Effects of dwell time on the fatigue life of Sn3.8Ag0.7Cu and Sn3.0Ag0.5Cu solder joints during simulated power cycling," *The Proceedings of the 57th Electr. Compon. Technol. Conf.*, Reno, Nevada, USA, May 29 - June 1, 2007, IEEE, (2007), pp. 227-234.

[76]   S. Chaparala, J. M. Pitarresi, and M. Meilunas, "Effect of dwell times and ramp rates on the thermal cycling reliability of Pb-free wafer- level chip scale packages: Experiments and modeling," *The Proceedings of ASME Inter. Mech. Eng. Congress & Exposition*, Chicago, IL, USA, Nov. 5-10, 2006, ASME, (2006), pp. 59-65.

[77] T. T. Mattila, J. Šimeček, and J. K. Kivilahti, "Failure modes of solder interconnections under mechanical shock loading at elevated temperatures," *The Proceedings of the 1st Electr. SystemIntegration Technol. Conf.*, Dresden, Germany, Sept. 5-7, 2006, IEEE, (2006), pp. 195-202.

[78] F. Y. Hung, T. S. Lui, L. H. Chen, and Z. F. Gu, "The recrystallization of microelectronic lead-free solders," *Mater. Trans.*, **49**, 10, (2008), pp. 2298-2302.

[79] J. J. Sundelin, S. T. Nurmi, and T. K. Lepisto, "Recrystallization behaviour of SnAgCu solder joints," *Mater. Sci. Eng. A*, **474**, 1-2, (2008), pp. 201-207.

[80] A. U. Telang, T. R. Bieler, A. Zamiri, and F. Pourboghrat, "Incremental recrystallization/grain growth driven by elastic strain energy release in a thermomechanically fatigued lead-free solder joint," *Acta Mater.*, **55**, 7, (2007), pp. 2265-2277.

[81] T.-M. K. Koehonen and L. P. Lehman, "Isothermal fatigue behavior of the near-eutectic Sn-Ag-Cu alloy between -25C and 125C," *J. Electr. Mater.*, **36**, 2, (2007), pp. 173-178.

[82] T. T. Mattila and J. K. Kivilahti, "Reliability of lead-free interconnections under consecutive thermal and mechanical loadings," *J. Electr. Mater.*, **35**, 2, (2006), pp. 250-256.

[83] T. Laurila, T. Mattila, V. Vuorinen, J. Karppinen, J. Li, M. Sippola, and J. K. Kivilahti, "Evolution of microstructure and failure mechanism of lead-free solder interconnections in power cycling and thermal shock tests," *Microelectr. Reliab.*, **47**, 7, (2007), pp. 1135-1144.

[84] C. Kanchanomai, Y. Miyashita, Y. Mutoh, and S. L. Mannan, "Influence of frequency on low cycle fatigue behavior of Pb-free solder 96.5Sn/3.5Ag," *Mater. Sci. Eng. A*, **345**, 1-2, (2003), pp. 90-98.

[85] C. Kanchanomai, Y. Miyashita, and Y. Mutoh, "Low cycle fatigue behavior and mechanisms of a Pb-free solder 96.5Sn-3.5Ag," *J. Electr. Mater.*, **31**, 2, (2002), pp. 142-151.

[86] Y. Kariya, T. Hosoi, S. Terashima, M. Tanaka, and M. Otsuka, "Effect of silver content on the shear fatigue properties of Sn-Ag-Cu flip-chip interconnects," *J. Electr. Mater.*, **33**, 4, (2004), pp. 321-328.

[87] R. Gagliano, G. Ghosh, and M. Fine, "Nucleation kinetics of Cu6Sn5 by reaction of molten tin with a copper substrate," *J. Electr. Mater.*, **31**, 11, (2002), pp. 1195-1202.

[88] J. Gong, C. Liu, P. P. Conway, and V. V. Silberschmidt, "Evolution of CuSn intermetallics between molten SnAgCu solder and Cu substrate," *Acta Mater.*, **56**, 16, (2008), pp. 4291-4297.

[89] R. Gagliano and M. Fine, "Growth of Cu6Sn5 phase scallops and whiskers in liquid tin-solid copper reaction couples," *JOM*, **53**, 6, (2001), pp. 33-38.

[90] W. G. Bader, "Dissolution of Au, Ag, Pd, Pt, Cu, and Ni in a molten tin-lead solder," *Weld. J. Res. Suppl.*, **28**, 12, (1969), pp. 551s-557s.

[91] P. G. Kim and K. N. Tu, "Morphology of wetting reaction of eutectic SnPb solder on Au foils," *J. Appl. Phys.*, **80**, 7, (1996), pp. 3822-3827.

[92] K. J. Zeng, V. Vuorinen, and J. K. Kivilahti, "Interfacial reactions between lead-free SnAgCu solder and Ni(P) surface finish on printed circuit boards," *IEEE Trans. Electr. Packag. Manuf.*, **25**, 3, (2002), pp. 162-167.

[93]   S. W. Chen and C. H. Wang, "Interfacial reactions of Sn-Cu/Ni couples at 250 °C," *J. Mater. Res.*, **21**, 9, (2006), pp. 2270-2277.

[94]   D. Q. Yu, C. M. L. Wu, D. P. He, N. Zhao, L. Wang, and J. K. L. Lai, "Effects of Cu contents in Sn–Cu solder on the composition and morphology of intermetallic compounds at a solder/Ni interface," *J. Mater. Res.*, **20**, 8, (2005), pp. 2205-2212.

[95]   D. R. Frear, J. W. Jang, J. K. Lin, and Z. Zhang, "Pb-free solders for flip chip interconnects," *JOM*, **53**, 6, (2001), pp. 28-33.

[96]   K. Nogita and T. Nishimura, "Ni-stabilized hexagonal (Cu,Ni)6Sn5 in Sn-Cu-Ni lead-free solder alloys," *Scr. Mater.*, **59**, (2008), pp. 191-194.

[97]   S. J. Wang and C. Y. Liu, "Study of interaction between Cu-Sn and Ni-Sn interfacial reactions by Ni-Sn3.5Ag-Cu sandwich structure," *J. Electr. Mater.*, **32**, 11, (2003), pp. 1303-1309.

[98]   H. Yu, V. Vuorinen, and J. K. Kivilahti, "Solder/substrate interfacial reactions in the Sn-Cu-Ni interconnection system," *J. Electr. Mater.*, **36**, 2, (2007), pp. 136-146.

[99]   Y. T. Chin, P. K. Lam, H. K. Yow, and T. Y. Tou, "Investigation of mechanical shock testing lead-free SAC solder joints in fine pitch BGA package," *Microelectr. Reliab.*, **48**, (2008), pp. 1079-1086.

[100]   K. J. Zeng, R. Stierman, T. C. Chiu, D. Edwards, K. Ano, and K. N. Tu, "Kirkendall void formation in eutectic SnPb solder joints on bare Cu and its effect on joint reliability," *J. Appl. Phys.*, **97**, 2, (2005), pp. 024508.

[101]   T.-C. Chiu, K. Zeng, R. Stierman, D. Edwards, and K. Ano, "Effect of thermal aging on board level drop reliability for Pb-free BGA packages," *The Proceedings of the 54th Electr. Compon. Technol. Conf.*, Las Vegas, NV, US, June 1-4, 2004, IEEE, 2, (2004), pp. 1256-1262.

[102]   A. Paul, "The Kirkendall effect in solid state diffusion," PhD Thesis, Eindhoven University of Technology, Eindhoven, The Netherland (2004).

[103]   K. N. Tu and R. D. Thompson, "Kinetics of interfacial reaction in bimetallic Cu-Sn thin films," *Acta Metall.*, **30**, 5, (1982), pp. 947-952.

[104]   V. Vuorinen, T. Laurila, T. Mattila, E. Heikinheimo, and J. Kivilahti, "Solid-state reactions between Cu(Ni) alloys and Sn," *J. Electr. Mater.*, **36**, 10, (2007), pp. 1355-1362.

[105]   W. Peng, E. Monlevade, and M. E. Marques, "Effect of thermal aging on the interfacial structure of SnAgCu solder joints on Cu," *Microelectr. Reliab.*, **47**, 12, (2007), pp. 2161-2168.

[106]   P. Borgesen, L. Yin, P. Kondos, D. W. Henderson, G. Servis, J. Therriault, J. Wang, and K. Srihari, "Sporadic degradation in board level drop reliability – Those aren't all Kirkendall voids!," *The Proceedings of the 57th Electr. Compon. Technol. Conf.*, Reno, Nevada, USA, May 29 - June 1, 2007, IEEE, (2007), pp. 136-146.

[107]   Y. Liu, J. Wang, L. Yin, P. Kondos, C. Parks, P. Borgesen, D. W. Henderson, N. Dimitrov, and E. J. Cotts, "Influence of plating parameters and solution chemistry on the voiding propensity at electroplated copper-solder interface, Part one: Plating in acidic copper solution with and without polyethylene glycol," *J. Appl. Electrochem.*, **38**, 12, (2008), pp. 1695-1705.

[108] L. Yin, P. Kondos, P. Borgesen, Y. Liu, S. Bliznakov, F. Wafula, N. Dimitrov, D. W. Henderson, C. Parks, M. Gao, J. Therriault, J. Wang, and E. Cotts, "Controlling Cu electroplating to prevent sporadic voiding in Cu3Sn," *The Proceedings of the 59th Electr. Compon. Technol. Conf.*, San Diego, California, USA, May 26-29, 2009, IEEE, (2009), pp. 406-414.

[109] J. Y. Kim and J. Yu, "Effects of residual impurities in electroplated Cu on the Kirkendall void formation during soldering," *Appl. Phys. Lett.*, **92**, 9, (2008), pp. 092109/1-3.

[110] J. Yu and J. Y. Kim, "Effects of residual sulphur on Kirkendall void formation at Cu/Sn–3.5Ag solder joints," *Acta Mater.*, **56**, 19, (2008), pp. 5514-5523.

[111] W. Q. Peng, "An investigation of Sn pest in pure Sn and Sn-based solders," *Microelectr. Reliab.*, **49**, 1, (2009), pp. 86-91.

[112] A. B. Kaufman, "Selecting solders for low temperature service," *Mater. Design Eng.*, **48**, 6, (1958), pp. 114-115.

[113] E. Cohen and A. K. W. A. van Lieshout, "Effect of mechanical deformation on the velocity of transformation of polymorphic metals. II. Effect of metallic additions. I," *Proc. K. Akad. Wet. Amsterdam*, **39**, (1936), pp. 352-358.

[114] E. Cohen and A. K. W. A. van Lieshout, "Effect of mechanical deformation on the velocity of transformation of polymorphic metals. III. Effect of metallic additions. II," *Proc. K. Akad. Wet. Amsterdam*, **39**, (1936), pp. 1174-1179.

[115] Y. Kariya, N. Williams, C. Gagg, and W.-J. Plumbridge, "Tin pest in Sn-0.5 wt.% Cu lead-free solder," *JOM*, **53**, 6, (2001), pp. 39-41.

[116] Y. J. Joo and T. Takemoto, "Transformation of Sn-Cu alloy from white tin to gray tin," *Mater. Lett.*, **56**, 5, (2002), pp. 793-796.

[117] M. Leodolter-Dworak, I. Steffan, W. J. Plumbridge, and H. Ipser, "Tin pest in Sn-0.5Cu lead-free solder alloys: A chemical analysis of trace elements," *J. Electr. Mater.*, **39**, 1, (2010), pp. 105-108.

[118] A. A. Matvienko and A. A. Sidelnikov, "The influence of relaxation of stresses occurring during the beta->alpha transformation of tin on the kinetics of the transformation," *J. Alloys Compd.*, **252**, 1-2, (1997), pp. 172-178.

[119] D. R. Flanders, E. G. Jacobs, and R. F. Pinizzotto, "Activation energies of intermetallic growth of Sn-Ag eutectic solder on copper substrates," *J. Electr. Mater.*, **26**, 7, (1997), pp. 883-887.

[120] J. Glazer, "Microstructure and mechanical properties of lead free solder alloys for low cost electronic assembly: a review," *J. Electr. Mater.*, **23**, 8, (1994), pp. 693-700.

[121] V. I. Igoshev, "Microstructure changes in Sn-3.5Ag solder alloy during creep," *J. Electr. Mater.*, **27**, 12, (1998), pp. 1367-1371.

[122] Y. Kariya and M. Otsuka, "Mechanical fatigue characteristics of Sn-3.5Ag-X (X = Bi, Cu, Zn and In) solder alloys," *J. Electr. Mater.*, **27**, 11, (1998), pp. 1229-1235.

[123] Y. Kariya and M. Otsuka, "Effect of bismuth on the isothermal fatifue properties of Sn-3.5 mass% Ag solder alloy," *J. Electr. Mater.*, **27**, 7, (1998), pp. 866-870.

[124] N.-C. Lee, "Getting ready for lead-free solders," *Sold. Surf. Mount Technol.*, **9**, 2, (1997), pp. 65-69.

[125] M. McCormack, S. Jin, and G. W. Kammlott, "The design of new, Pb-free solder alloys with improved properties," *The Proceedings of Inter. Symp. Electronics and Environment*, Orlando, FL , USA, May 1-3, 1995, IEEE, (1995), pp. 171-176.

[126] C. Melton, "Nitrogen atmosphere processing in lead-free soldering," *The Proceedings of Technical Program, NEPCON WEST '95*, Norwalk, USA, 1995, Vol. 2, (1995), pp. 1003-1011.

[127] W. J. Plumbridge, "Solder in electronics," *J. Mater. Sci.*, **31**, 10, (1996), pp. 2501-2514.

[128] D. Shangguan and A. Achari, "Lead-free solder development for automotive electronics packaging applications," *The Proceedings of Surface Mount Inter., Advanced Electr. Manuf. Technol.*, San Jose, CA, USA, August 1995, SMTA, (1995), pp. 423-428.

[129] Z. Guo and G. J. Thomas, "Strengthening and dragging characteristics of dilute Sn solders designed for electronic packages," *The Proceedings of ASME Inter. Mech. Eng. Congress & Exposition*, Atlanta, GA, USA, Nov. 17-22, 1996, ASME, (1996), pp. 179-196.

[130] F. Hua and J. Glazer, "Lead-free solders for electronic assembly," *The Proceedings of Design and Reliability of Solders and Solder Interconnections*, Orlando, Florida, USA, Feb. 10-13, 1997, Minerals, Metals and Materials Society/AIME, (1997), pp. 65-73.

[131] Y. Nakamura, "Microstructure of solder joints with electronic components in lead-free solders," *Sold. Surf. Mount Technol.*, **10**, 1, (1998), pp. 10-12.

[132] M. McCormack and S. Jin, "Progress in the design of new lead-free solder alloys," *JOM*, **45**, 7, (1993), pp. 36-40.

[133] M. McCormack and S. Jin, "New Pb-free solders," *J. Electr. Mater.*, **23**, 7, (1994), pp. 635-640.

[134] M. McCormack, S. Jin, H. S. Chen, and D. A. Machusak, "New Pb-free, Sn-Zn-In solder alloys," *J. Electr. Mater.*, **23**, 7, (1994), pp. 687-690.

[135] S. W. Yoon, J. R. Soh, B.-J. Lee, and H. M. Lee, "Alloy design of Sn-Zn-X (X=In, Bi) solder systems through phase equilibria calculations," *The Proceedings of Design and Reliability of Solders and Solder Interconnections,*, Orlando, Florida, USA, Feb. 10-13, 1997, Minerals, Metals and Materials Society/AIME, (1997), pp. 121-128.

[136] P. Harris, M. Whitmore, R. Billington, T. Harman, C. Tanner, B. Richards, J. Vincent, H. Steen, and M. Warwick, "Pb-free solders for electronic assemblies," Report, International Tin Research Institute (1998).

[137] A. Z. Miric, "Lead-free alloys," *Sold. Surf. Mount Technol.*, **10**, 1, (1998), pp. 19-25.

[138] K. Nimmo, "Review of current issues in lead-free soldering," *The Proceedings of Surface Mount Inter. (SMI '97)*, San Jose, California, USA, Sept. 7-11, 1997, SMTA, (1997), pp. 467-475.

[139] H. Yu, "Combined thermal, thermodynamic and kinetic modeling for the reliability of high-density lead-free solder interconnections," PhD Thesis, Helsinki University of Technology, Helsinki, Finland (2006).

[140] I. Anderson, "Sn-Ag-Cu: A lead-free solder for board applications," *The Proceedings of NEPCON West '96*, Anaheim, CA, USA, Feb. 27-29, 1996, Reed Exhibition, 2, (1996), pp. 882-887.

[141] C. M. Miller, I. E. Anderson, and J. F. Smith, "A viable Sn-Pb solder substitute: Sn-Ag-Cu," *J. Electr. Mater.*, **23**, 7, (1994), pp. 595-601.

[142] D. R. Frear, "The mechanical behavior of interconnect materials for electronic packaging," *JOM*, **48**, 5, (1996), pp. 49-53.

[143] B. P. Richards, "Tomorrow's solder today," http://www.alphametals.com

[144] E. Gebhardt and G. Petzow, "Constitution of the Ag-Cu-Sn system," *Z. Metallkde.*, **50**, 10, (1959), pp. 597-605.

[145] D. Cavasin, "The impact of interfacial void formation on Pb-free Sn-4.0Ag-0.5Cu BGA solder joint integrity," *The Proceedings of the 56th Electr. Compon. Technol. Conf.*, San Diego, CA, USA, May 30 - June 2, 2006, IEEE, (2006), pp. 1191-1195.

[146] JESD22-B111, "Board level drop test method of components for handheld electronic products," JEDEC Solid State Technology Association, 2003, 16 p.

[147] JESD22-A104C, "Temperature cycling," JEDEC Solid State Technology Association, 2005, 12 p.

[148] W. Weibull, "A statistical distribution function of wide applicability," *J. Appl. Mech.*, **18**, 9, (1951), pp. 293-297.